A best-case probe, light source, and database for H_2O absorption thermometry to 2100 K and 50 bar.

by

Mack S. Brittelle

A dissertation submitted in partial fulfillment of

the requirements for the degree of

Doctor of Philosophy

(Mechanical Engineering)

at the

UNIVERSITY OF WISCONSIN-MADISON

2017

Date of final oral examination: 12/21/2016

The dissertation is approved by the following members of the
Final Oral Committee:
      Scott Sanders, Professor, Mechanical Engineering
      Dave Rothamer, Associate Professor, Mechanical Engineering
      Jaal Ghandhi, Professor, Mechanical Engineering
      Sage Kokjohn, Assistant Professor, Mechanical Engineering
      Mark Anderson, Research Professor, Engineering Physics

Abstract

A best-case probe, light source, and database for H_2O absorption thermometry to 2100 K and 50 bar.

Mack S. Brittelle

Under the supervision of Professor Scott Sanders

At the University of Wisconsin-Madison

This work aspired to improve the ability of forthcoming researchers to utilize near IR H_2O absorption spectroscopy for thermometry with development of three best-case techniques: the design of novel high temperature sapphire optical access probes, the construction of a fixed-wavelength H_2O absorption spectroscopy system enhanced by an on-board external-cavity diode laser, and the creation of an architecture for a high-temperature and -pressure H_2O absorption cross-section database. Each area's main goal was to realize the best-case for direct absorption spectroscopy H_2O vapor thermometry at combustion conditions.

Optical access to combustion devices is explored through the design and implementation of two versions of novel high-temperature (2000 K) sapphire immersion probes (HTSIPs) for use in ambient flames and gas turbine combustors.

The development and evaluation of a fixed wavelength H_2O absorption spectroscopy (FWAS) system that is demonstrates how the ECDL allows the system to operate in multiple modes that enhance FWAS measurement accuracy by improving wavelength position monitoring, and reducing non-absorption based contamination in spectral scans.

The architecture of a high temperature (21000 K) and pressure (50 bar) database (HTPD) is developed that can enhance absorption spectroscopy based thermometry. The HTPD formation is developed by the evaluation of two approaches, a line-by-line (LBL) approach, where

transition lineshape parameters are extracted from spectra and used along with a physics based model to allow the simulation of spectra over a wide range of temperatures and pressures, or an absorption cross-section (σ_{abs}) approach, where spectra generated from a high temperature and pressure furnace are catalog spectra at various conditions forming a database of absorption cross-sections that is then interpolated to provide a simulated absorbance spectra based on measured reference grade spectra. Utilizing near future reference grade H_2O absorption spectra, generated by the Sanders Group by means of an ECDL and a high temperature and pressure furnace, a unique opportunity is taken to provide the research community with a database that can be utilized for optical thermometry.

Acknowledgment

This effort would not have been possible without the direction provided by my advisor, Scott Sanders. I would like to thank him for providing me the opportunity to be one of his graduate students, introducing me to the field of spectroscopy, and supplying me with challenging, novel, and large budget projects.

I am forever grateful to Kelly Burton and all of the GERS community for their willingness to create opportunity and provide both financial and personal support for their students.

Special thanks to my fellow Sanders group members, both past and present, for their valuable advice and willingness to share knowledge. I would like to specifically thank Scott Melin for insightful discussions and Ze Wang for his enthusiasm to provide assistance.

I would like to thank my parents, my mother for instilling a never give up attitude, which became heavy relied upon during my time at the University, and my late father for always reminding me about what is important, which he best exemplified through a Frank Lloyd Wright quote, "A great Architect is not made by way of a brain nearly so much as he is made by way of a cultivated, enriched heart."

Most Importantly, I am beholden to my future wife Samantha, who enriched my academic career and continues to better our life through her unwavering love, support, and friendship.

Table of Contents

List of Tables

List of Equations

List of Figures

Nomenclature

Term	Abbreviation
absorption cross-section	σ_{abs}
acousto-optic modulator	AOM
adhesive-free bond	AFB
amplified spontaneous emission	ASE
arbitrary waveform generators	AWG
differential-evolution genetic-algorithm	DE-GA
distributed feedback laser	DFB
external cavity diode laser	ECDL
fixed wavelength absorption spectroscopy	FWAS
free spectral range	FSR
Fourier-transform infrared	FTIR
frequency division multiplex	FDM
Gaussian white noise	GWN
high temperature and pressure database	HTPD
high-temperature sapphire immersion probe	HTSIP
Hydrogen fluoride	HF
line-by-line	LBL
Mach-Zehnder interferometer	MZI
polarization-maintaining	PM
root mean square	RMS
semiconductor optical amplifier	SOA

signal-to-residual ratio	SRR
signal-to-noise ratio	SNR
thermal electric cooler	TEC
time division multiplex	TDM
tunable diode-laser absorption spectroscopy	TDLAS
variable optical attenuator	VOA
wavelength stabilized distributed feedback laser	WSDFB

Chapter 1. Thesis structure

I begin this dissertation by introducing, in Chapter 2, optical access to combustion devices exploring the design and implementation of two versions of novel high-temperature (2000 K) sapphire immersion probes (HTSIPs) for use in ambient flames and gas turbine combustors. In Chapter 3, I describe the design and evaluation of a fixed wavelength H_2O absorption spectroscopy (FWAS) system that is enhanced by an on-board External Cavity Diode Laser (ECDL). The ECDL allows the system to operate in multiple modes that enhance FWAS measurement accuracy by improving wavelength position monitoring, and reducing non-absorption based contamination in spectral scans. The final chapter, Chapter 4, discusses the architecture of a high temperature and pressure database (HTPD) that can enhance absorption spectroscopy based thermometry. The HTPD formation is established by the evaluation of two approaches, a line-by-line (LBL) approach, where transition lineshape parameters are extracted from spectra and used along with a physics based model to allow the simulation of spectra over a wide range of temperatures and pressures, or the absorption cross-section (σ_{abs}) approach, where spectra generated from a high temperature and pressure furnace are catalog spectra at various conditions forming a database of absorption cross-sections that is then interpolated to provide a simulated absorbance spectra at any condition inside of our measured test matrix, and is founded on measured spectra.

Chapter 2. Optical access

2.1   Motivation

Optical techniques have become ubiquitous in the field of combustion research. Some techniques require the creation of one or more optical ports in surfaces, which act as temperature and pressure barriers. In several cases optical ports can be as simple as solid windows. An alternative approach described by Fateev and Clausen [1] employs laminar flow boundaries as a window substitute, however these gas boundaries may be difficult to implement on test articles with transient pressures. Traditional laser based H_2O absorption spectroscopy techniques require line-of-sight optical access. The objective of this chapter is to describe opportunities for H_2O absorption spectroscopy using only a single optical access port.

2.2   Probe access background

Traditional line-of-sight optical access (also known as through-, double-port-, or two-sided-access), allows for light to be transmitted from one side of the test volume and received on the other. Line-of-sight access is often a default approach due to its low complexity and high throughput. Line-of-sight access may not be available in some test articles such as gas turbine combustors, which have limited access for a beam to be transmitted radially. In these situations, one option is to use the geometry employed by Smith [2] to create a probe with two adjacent ports. This probe is formed using two parallel sapphire rods immersed in the test gas. Each immersed rod end has a 45-degree polished flat used as a total internal reflection mirror. A second polished flat is adjacent to each 45-degree flat to allow the sensor light to transition into / out of the test gas. Regrettably, long sapphire rods can absorb a significant fraction of the infrared (IR) sensor light at elevated temperatures as shown by Gryvnak et al. [3].

An alternative approach is desired to implement absorption spectroscopy with single-port, single-sided optical access in high temperature gases. A single-port probe is convenient for use in numerous practical test articles. The laser is transmitted and received from the same access port requiring the light to be redirected by scattering off test volume surfaces, or reflecting off a mirror suspended and immersed in the test gas. Wang has recently demonstrated a wavelength modulated absorption spectroscopy probe [4] that transmits a beam onto a rough surface and detects the light scattered off the rough surfaces from the same port. Unfortunately, the throughput for this backscatter approach is typically ~ 1 ppm, leading to low signal-to-noise ratio.

Commercial immersion probes, such as the one produced by LaVision GmbH [5], have been proven successful operating at 30kHz in internal combustion engine. The LaVision probe uses an IC engine spark plug port for access. The probe integrates an optical probe next to fully functioning spark plug electrodes, in the same space a standard spark plug occupies, as shown in Figure 2.1.
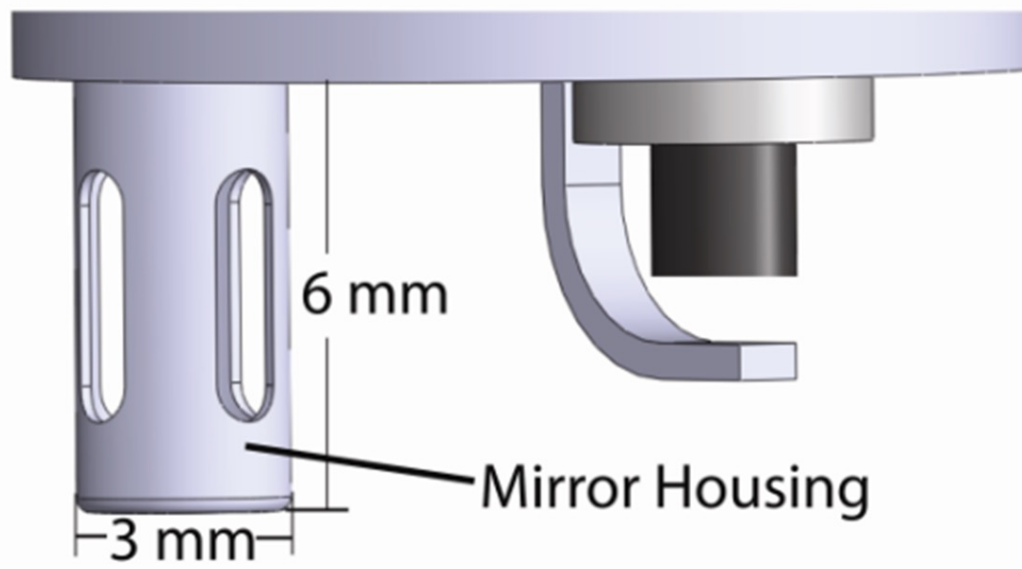
Figure 2.1 LaVision spark plug probe: optical probe on left, spark plug electrodes on the right

Sapphire windows transmit and receive the light that is reflected off a metallic spherical mirror suspended into the engine cylinder by a perforated tube, allowing for the mirror and optical path to be immersed into the test gas. Our goal is to use the suspended mirror immersion geometry, but in a design that allows the mirror to operate at 2000 K without degradation.

2.3 High-temperature sapphire immersion probe Version 1: multi-bond

Version 1 of the high-temperature sapphire immersion probe (HTSIP) is designed for high temperature (2000 K) atmospheric flame H_2O absorption thermometry. The high temperatures require a material that can withstand 2000 K while maintaining transparency throughout the IR region. With a melting point of ~2300 K, sapphire is an obvious choice. However, due to the elevated temperatures, adhesive bonding was not feasible. Adhesive-free bonding performed by Onyx Optics, Inc. permits multiple sapphire crystals to be bound together forming a monolithic crystal sapphire probe. The adhesive-free bond (AFB) utilizes the Van der Waals forces that attract extremely flat surfaces together. Version 1 of the HTSIP is ~88 mm long with an 8 mm x 8 mm square cross section as illustrated in Figure 2.2. All sapphire crystal segments have the crystal c-axis aligned parallel to the long axis of the completed probe.
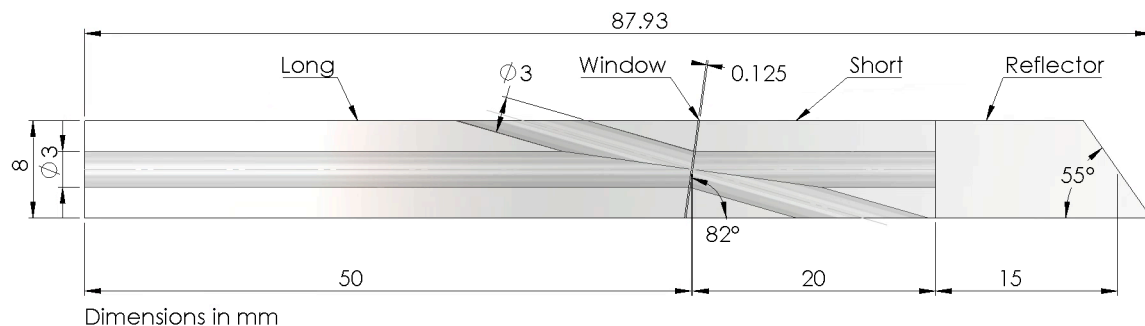
Figure 2.2 High-temperature sapphire immersion probe version 1

The HTSIP is constructed out of four crystals, named as follows: long, window, short section, and reflector. The long (50 mm) and short (20 mm) sections are identical except for the lengths;

both have one perpendicular end facet while the opposite end facet is angle-polished 82 degrees from the optical axis. A 3 mm bore, along the optical axis, passes through the long and short sections; a 3 mm bore, angled 16 degrees off the optical axis, intersects the previous optical axis bore at the angled-polished facet. The angled ports function primarily as the gas sampling port for the short section, and as the purge outlet for the long section. Secondarily, the angled ports allow stray reflections produced by the window to be dumped away from the probe. The first AFB joins the polished facet of a thick window (> 4 mm) to the angle-polished facet of the short section. The window is polished to the final thickness of 125 microns. A second AFB joins the angle-polished facet of the long section to the thin window. The third and final AFB is made between the perpendicular facet of the short section and the perpendicular facet of the reflector. The reflector is a ~15 mm long cube prism with one perpendicular end facet and the opposite end facet angle-polished 55 degrees from the optical axis, acting as a beam trap for stray light transmitted into the reflector.

The HTSIP operates as follows:

- The HTSIP is immersed in a test gas (such that hot gases heat at least the window, short, and reflector sections)

- Test gas H_2O vapor fills the short section. Hot H_2O vapor would also start filling the long section, however this bias is removed by purging the long section with dry nitrogen.

- Light is directed through the window, partially absorbed by the H_2O vapor in the short section bore, and reflected off the reflector facet back upstream to be detected.

The 125-micron thick window will produce an optical interference pattern called an etalon. The etalon is caused by multiple reflections from the two parallel surfaces. The successive reflected optical intensity maxima have a wavelength separation called the free spectral range (FSR). The FSR is given by

$$FSR(v,T) = \frac{1}{2n(v,T)\ell(T)}$$

Equation 2.1 Free spectral range

Where n is the temperature- and wavenumber-dependent index of refraction and ℓ is the temperature-dependent window thickness. I plan to use the FSR of the window for secondary thermometry of the HTSIP window. To calibrate the window's etalon, the FSR will be measured at different temperatures using the following test. The HTSIP will be placed inside a furnace and an ECDL will be used to measure spectra at different temperatures. Collected data will be post-processed until the etalon signal is reduced to wavelength-dependent FSR values at each temperature. This measurement will then be compared to the model developed by Yang [6]. Figure 2.3 shows Yang's model of the expected FSR verses temperature for a 125-micron thick window measured at 7462 cm^{-1}.
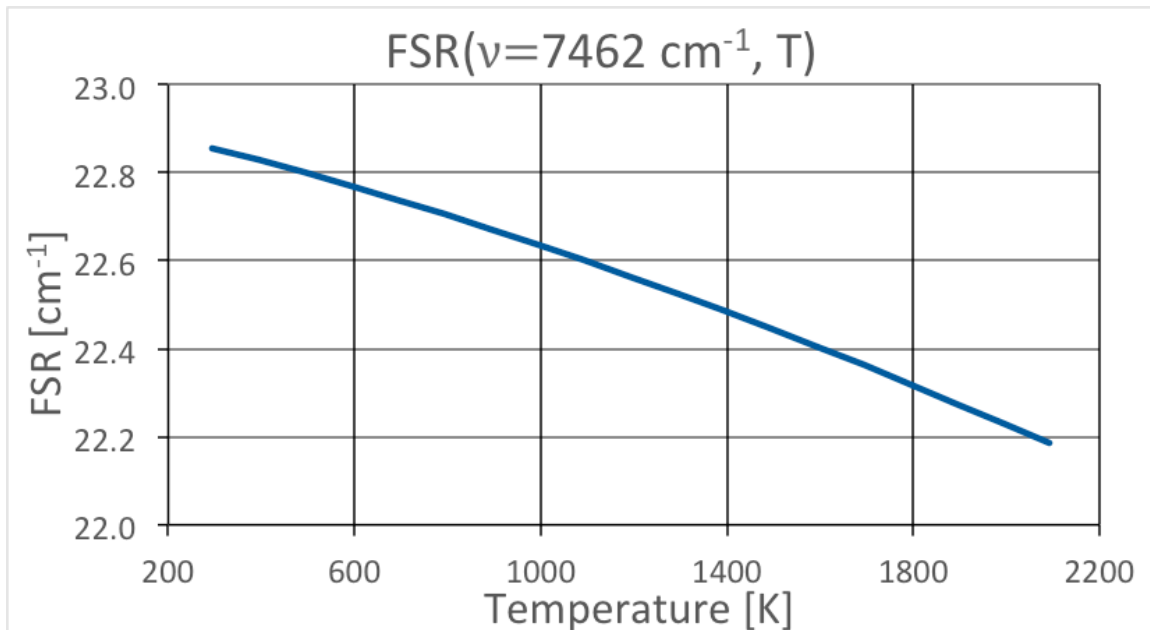
Figure 2.3 FSR verses temperature at 7462 cm^{-1} based on Yang's model.

The probes ability to recover the FSR of the etalon was tested, and future work is planned to be carried out on version 2.

2.4 High-temperature sapphire immersion probe version 2: single-bond

The second version of the HTSIP is designed to operate immersed in gas turbine combustor test articles. The manufacturing (machining, polishing, and bonding) of sapphire crystals for version 1 was found to be an expensive and slow process. In order to increase development productivity, a second configuration was designed to reduce manufacturing time, cost, and the response time of version 1.
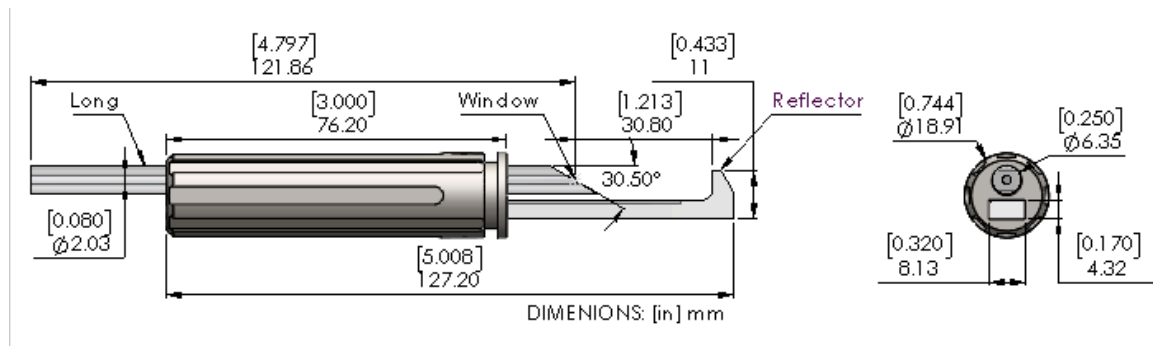
Figure 2.4 High-temperature sapphire immersion probe version 2

Version 2 of the HTSIP has been designed and is in the process of being manufactured. The HTSIP version 2 removes the short section and its two associated AFBs, separating the long section and window from the reflector. The reflector is a single ~127 mm long x ~8 mm wide x 14 mm tall piece of sapphire shaped like an L. The inside perpendicular polished facet acts as the reflective surface. The long section is now constructed from a stock sapphire tube with an OD of ~6 mm and an ID of ~2 mm. The tube is polished at Brewster's angle. The tube part is ~121 mm long overall. The single remaining AFB connects the 125-micron thick window at Brewster's angle (30.5 degrees from the optical axis) to the tube. The window is bonded at Brewster's angle

to reduce the strength of the etalon contamination found in the signal used for absorption spectroscopy. Residual etalon contamination will still be used for solid (window) thermometry. The long section with the Brewster window will be fixtured in a 6-mm-diameter circular through bore made in a ~19-mm-diameter x 76-mm-long stainless steel sleeve. The reflector will be fixtured into a blind 8 mm x 4 mm rectangular bore in the same sleeve. Cooling channels are machined into the outside of the sleeve. This stainless steel sleeve is then welded into a double-wall stainless steel tube. Cooling water flows through the region between the tube walls. The inner aperture of the tube is open, allowing laser access to the reflector; this aperture is purged with dry nitrogen. Version 2 is slated to complete manufacturing in the coming months. It will then be initially tested by the United States Air Force in an evaluation rig and then further implemented in a gas turbine combustor to evaluate the thermometry performance.

Chapter 3. Fixed-wavelength H$_2$O absorption spectroscopy system enhanced by an on-board external-cavity diode laser

3.1 Motivation

Tunable diode-laser absorption spectroscopy (TDLAS) has been widely successful in measuring gas properties in practical combustion systems such as industrial burners [7], gas turbine combustors [8], and reciprocating engines [9]. These combustion systems often require measurements at rates of 10 kHz or greater. In this paper we focus on the measurement of H$_2$O vapor temperature and mole fraction, although extension to other species is straightforward. Much of the previous TDLAS work has involved acquisition of spectra, usually with scanned-wavelength distributed feedback lasers (DFB) (e.g. Arroyo et al. [10]), but sometimes with swept-wavelength lasers offering broader spectral coverage (e.g. Witzel et al. [11] and Kranendonk et al. [12]). Often, measurement repetition rates are in the range of 10–30 kHz, and each repetition typically involves ~1000 wavelength data points, demanding data acquisition rates of roughly 10–30 MHz. At these rates, signal-to-noise (SNR) ratios can suffer, data acquisition equipment can be expensive, and file sizes can become large. These problems are often exacerbated by low throughput and by multiple beams as in the case of tomography [8]. Furthermore, some situations demand even higher repetition rates (e.g., for measurements in detonation devices, repetition rates of ≥100 kHz are often desired). Another gas sensing approach that lends itself to high-speed measurements is fixed wavelength absorption spectroscopy [13-17]. These systems record individual wavelength data points instead of thousands, tending to improve SNR, reduce cost, and decrease file size. In addition, FWAS is simpler; for example, the need to map wavelength sweeps from time to wavelength, using

references such as etalons, is eliminated. Finally, to combat low throughput, FWAS is better suited to amplification: amplifier gain bandwidth can be narrow, and amplified spontaneous emission (ASE) can be rejected if needed by spectral bandpass filtering. Work done by An et al. [18] stated that electing to measure two wavelengths, as an alternative to measuring all wavelengths (i.e. a scanning approach), increases the temperature precision by ~15 times. However, the limited spectral information measured in FWAS brings its own challenges: FWAS is more sensitive to spectral modeling errors and to variations in the zero-absorption baseline. This paper details a FWAS system that includes an external cavity diode laser (ECDL) to assist in addressing FWAS challenges. In addition to the ECDL benefits, this work extends the work of Karagiannopoulos et al. [16] by improving aspects such as wavelength locking with reference features and elimination of amplifier ASE.

3.2   Method

3.2.1   Ratiometric measurements

Ratiometric spectroscopy is the primary thermometry method for FWAS. Ratiometric measurements have been thoroughly described theoretically [10, 19] and also experimentally executed in combustion environments [19-21]. A common and preferred approach involves measurements at three wavelengths [20]: two H_2O-resonant wavelengths and one baseline wavelength. The baseline wavelength is chosen near a H_2O absorption minimum, and is used to track contamination (e.g., losses due to beamsteering). The H_2O-resonant wavelengths are chosen such that the ratio of their molecular absorbance values is temperature sensitive. The Beer-Lambert-Bouguer law is used to convert transmission measurements at each wavelength to absorbance. The baseline wavelength absorbance is subtracted from each of the two H_2O-resonant absorbance values, reducing contamination. The ratio of the two

baseline-corrected results is computed; temperature is then inferred by comparing the measured ratio to reference data. Reference data is generally simulated using a spectroscopic database (e.g., HITRAN2012 [22] or HITEMP2010 [23]). Using the measured temperature, H_2O mole fraction can then be inferred by comparing simulated reference absorbance values with measured absorbance values.

3.2.2 Spectral modeling

Accurate FWAS relies on having accurate H_2O absorption reference data. For humid air near standard temperature and pressure, HITRAN2012 [22] models agree well with experimental spectra; for example, a recent study [24] revealed line position errors in atmospheric spectra of $\leq$ 80 MHz. Accordingly, FWAS is typically well-suited to accurate thermometry of gases at ordinary conditions. However, model accuracy degrades with increasing temperature. Alberti et al. [25] found that, relative to a H_2O spectrum recorded at 1770 K, a HITEMP2010 [23] simulation exhibits a residual of 45% (calculation based on Figure 42 [25] near 7203 cm^{-1}).

We generally use a standard application [26] of HITEMP2010 to model the spectra of combustion gases, and commonly observe disagreement with natural spectra. There are many sources for the discrepancies. First, HITEMP2010 lacks data such as H_2O-CO_2 broadening coefficients, so we approximate results using H_2O N_2 coefficients for both H_2O-CO_2 and H_2O-N_2. Second, the standard application [26] ignores line mixing, which can become significant at high pressures as shown by Farooq [27]. Finally, the errors in the existing HITEMP2010 data can be significant. In this paper, initial experiments are carried out near room conditions, even though the system was designed to monitor gases over a range of combustion-relevant conditions (800 K to 2100 K and 1 to 30 bar). Improvements in reference spectra are needed before satisfactory results can be obtained at those conditions. We expect that

a FWAS system that performs well at room conditions will later perform well at combustion conditions, once improved reference spectra are available. Several groups are currently working to collect suitable reference spectra [24, 25, 28].

3.2.3 High temperature and pressure spectral feature selection

Many wavelength-selection procedures have been previously used [29-31]. In this paper, the wavelength selection procedure described by An et al. [18] was selected. Table 3.1 notes the chosen wavelengths and their intent.

Table 3.1 Selected measurement wavelengths, optimized for measurements of H_2O gas temperature and mole fraction for temperatures in the range of 800 – 2100 K and total pressures in the range of 1 – 30 bar.

Laser Source	Measured λ [nm]	Modulating Frequency [MHz]	Spectroscopic H_2O Feature	Reference Element
λ1	1321.253	0.893	Baseline	HF Cell
λ2	1346.900	0.926	Hot, Far Wing	Etalon
λ3	1347.830	0.962	Hot, Near Wing	Etalon
λ4	1348.105	1.000	Hot, Peak	H_2O cell
λ5	1364.689	1.042	Cold, Peak	H_2O cell
λ6	1364.724	1.087	Cold, Near Wing	Etalon
λ7	1366.059	1.136	Cold, Far Wing	Etalon
ECDL	1320-1368	1.190	Full Scan	-

Wavelength λ1 is located on a Hydrogen Fluoride (HF) absorption peak. Wavelengths λ2- λ7 were selected for their temperature and pressure sensitivity over a range of conditions (800 K to 2100 K and 1 to 30 bar). The two main H_2O-resonant wavelengths, λ4 and λ5, are located on temperature-sensitive absorption peaks. Wavelength λ4 is located near the peak of a hot H_2O

absorption feature: a feature that is relatively stronger at high temperature. Wavelength $\lambda 5$ is located near the peak of a cold H_2O absorption feature: a feature that is relatively stronger at low temperature. These temperature-sensitive peaks are used for ratiometric thermometry measurements. At atmospheric pressures, the baseline wavelength, $\lambda 1$, experiences negligible absorption due to water vapor. Even at high temperature (2100 K) and pressure (30 bar), the simulated $\lambda 1$ absorbance value is ~120 times smaller than the $\lambda 5$ absorbance, making the associated error negligible. Wavelengths $\lambda 2$, $\lambda 3$, $\lambda 6$, and $\lambda 7$, located on the wings of corresponding peaks $\lambda 4$ and $\lambda 5$, were assigned to monitor variations in the lineshape caused by pressure broadening and line mixing. For pressure-broadened measurements, the ratio of absorbances between peak and wing wavelengths can be used to infer pressure or assist in adjusting broadening coefficients to match simulated spectra to measured spectra.

3.3   Opto-electronic setup

3.3.1   Laser sources

Accurate FWDAS measurements rely on precise laser wavelength control. The system uses seven wavelength stabilized distributed feedback (WSDFB) lasers $\lambda 1$-$\lambda 7$ (Wavelength References, Clarity) and one tunable external cavity diode laser (ECDL, New Focus TLB-6600). Figure 3.1 displays the schematic diagram of the laser system. All fiber-based optical components in this system were constructed using polarization-maintaining (PM) fiber (Fujikura PANDA SM13-PS-U25A or equivalent). PM fiber was chosen for improved stability as described in Section 3.3.2 - 3.3.4 below.
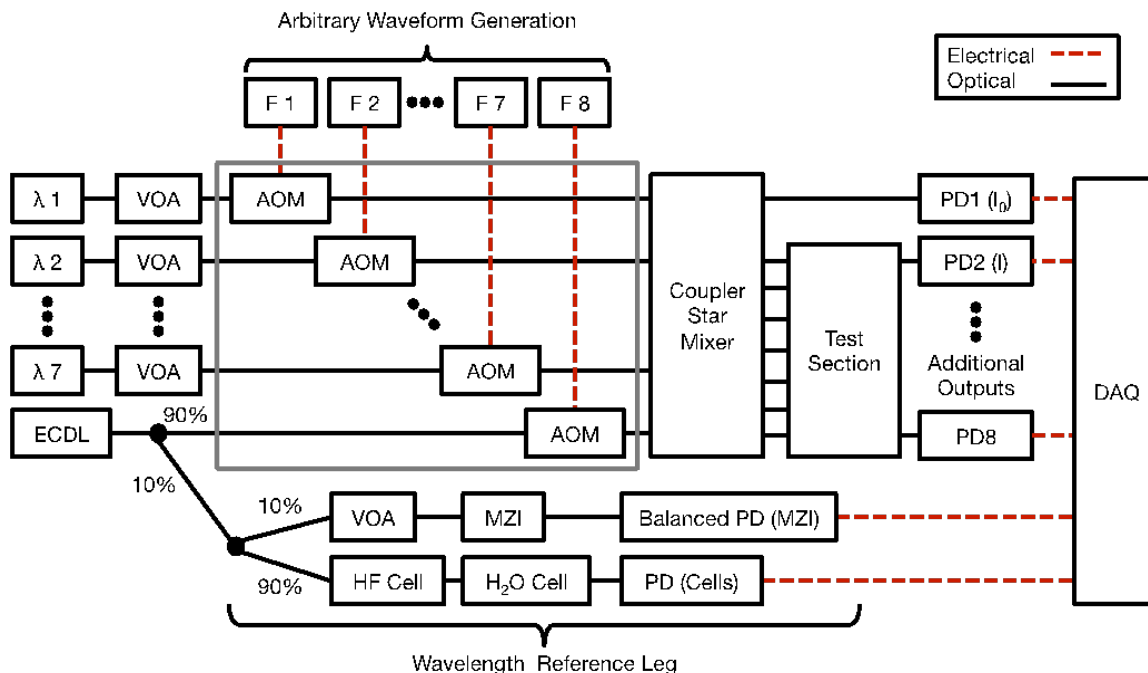
Figure 3.1 Opto-Electronic schematic of the laser system. Seven fixed wavelengths (λ1- λ7) and one low-speed swept wavelength (ECDL) are each modulated by one of eight independent acousto-optic modulators (AOM).

Each WSDFB laser is based on a 20 mW DFB laser (NTT Electronics, NLK1B5GAAA & NLK1E5GAAA) optically coupled to a wavelength reference element. Electronic wavelength circuitry within each WSDFB laser unit maintains the wavelength stability at ±1 MHz. We used four Zerodur etalons (Primanex, PETL1-211T21200), two low-pressure (10 Torr) H_2O vapor cells (Wavelength References, H2O–H(16.5)–10), and one low-pressure (10 Torr) HF vapor cell (Wavelength References, HF–H(2.7)–10) as wavelength reference elements. We selected seven etalons from a lot of 20 etalons purchased; after down-selection, each etalon had a transmission peak within 0.08 cm^{-1} of the desired wavenumber. A photodiode within each WSDFB unit monitors the transmission through the gas cell or etalon; a 500Hz dual-loop control configuration then adjusts the laser current bias and thermal electric cooler (TEC) temperature, in order to cause the laser wavelength to shift back to the center of the peak maintaining the wavelength stability to ±1 MHz. The ECDL utilizes a modified Littman–Metcalf configuration, provides

1 mW output, and tunes over a range of 1320 – 1365 nm at rates of 2 to 2000 nm/s. Each of the seven WSDFB lasers output directly to PM variable optical attenuators (VOAs), allowing for the optical power to be balanced across all wavelengths. The ECDL is not attenuated by a VOA because of its relatively low power.

3.3.2   Multiplexing

Acousto-optic modulators (AOM, Brimrose, AMM-55) are used to modulate the optical power of each laser. AOMs were chosen over semiconductor optical amplifiers (SOAs) as used previously [10] because AOMs do not add ASE. Analog electronic signals used to modulate the RF drivers (Brimrose, FFE-55) were generated by two four-channel arbitrary waveform generators (AWG, Tabor Electronics, WW1074).

All eight AOM outputs were combined using an 8x8 PM fiber-optic passive mixing star coupler such that each output of the star includes approximately equal portions of all eight unique inputs. The star topology allows for interference-free mixing as well as low insertion loss, in this case 8 dB theoretical loss +1 dB excess loss = 9 dB total loss. PM fiber ensures split ratios that do not vary significantly with fiber handling or temperature. Of the eight star outputs, one is intended for use as a reference beam intensity (Io), and the seven others as sensor beams, e.g., beams used to monitor different locations in a test section.

3.3.3   Signal acquisition

The system contains two custom detector assemblies: one in the wavelength reference leg, PD (Cells), and the other at the end of the multiplexed reference fiber, PD1 (Io). Each assembly is made by gluing a PM fiber to a photodiode (GPD Optoelectronics Corp., GAP544) as described by Whitney [32] and subsequently inserting the photodiode into a fixed-gain amplifier (Thorlabs,

PDA10\CF, modified PDA10CF without photodiode). All photodiode outputs were fed to a 60MS/s, 8-channel data acquisition card (National Instruments, PXI-5051).

3.3.4 Absolute wavelength reference

We used a PM Mach-Zehnder interferometer (MZI) in conjunction with low-pressure vapor cells to reference our signals to absolute wavelength, as shown in the Wavelength Reference Leg portion of Figure 3.1. Prior to multiplexing, the ECDL output is split; 90% is directed to the AOM while 10% is directed to the wavelength reference leg. The wavelength reference leg is split again; 10% is directed through a VOA and MZI, while 90% is directed through two gas reference cells in series. The MZI has a nominal FSR of 90 MHz. The MZI is operated within an ice water bath to stabilize its temperature, and, in turn, its FSR. The MZI output signal is converted to an electrical signal by a balanced detector (Thorlabs, PDB130C) and recorded with the data acquisition system. A low-pressure (10 Torr) 3-cm-long Hydrogen fluoride (HF) vapor cell (Wavelength References, HF–H(2.7)-10) is connected in series with a 16.5-cm-long cell containing low-pressure (10 Torr) H_2O (Wavelength References, H2O–H(16.5)-10). In an initial ECDL scan, a HF absorption peak near the start of the scan (MZI 1) and a H_2O peak near the end of the scan (MZI 2), indicated in Figure 3.2a, are identified. These two peaks are assigned spectral positions according to HITRAN2012 [22]. The FSR of the MZI is then computed as the spectral difference between the HF and H_2O peaks divided by the number of MZI fringes measured between the HF and H_2O peaks. Then, for all future scans, measurement of the HF peak provides absolute wavelength, and measurement of the MZI trace provides relative wavelength, so that the entire ECDL scan can be mapped to absolute wavelength.

3.3.5 Optical access to test environments

For results presented in Section 3.5, before the light is transmitted across a given test section, it is collimated from a PM FC/APC fiber using a FC/APC coupled off-axis parabolic reflective mirror (Thorlabs, RC02APC-P01). After traveling through the test section the transmitted beam is focused using a plano-convex lens (Thorlabs, LA1213). The focused beam is detected using a photodiode in a package without a window (GPD, GAP 544); the photodiode signal is in turn amplified by a fixed gain amplifier (Thorlabs, PDA10\CF).

3.4 Modes

This system can operate in numerous modes to allow for various test conditions and objectives. Five modes are listed below. The first mode is a system diagnosis mode; the remaining four modes are for gas sensing:

- Heterodyne: WSDFB wavelength position monitoring

- Spectrum-lab: ECDL scan to obtain reference H_2O spectra

- Frequency Division Multiplex (FDM): simultaneous measurement of seven fixed wavelengths for measurements of gas temperature and H_2O mole fraction

- Spectrum-field: Use baseline WSDFB laser to monitor interferences such as beam steering to correct ECDL swept spectrum measurements

- Time Division Multiplex (TDM): simultaneous measurement of seven fixed wavelengths, as in FDM, but here by turning each WSDFB laser on and off one at a time in rapid succession

3.4.1   Heterodyne

A mode is developed for this system that monitors the absolute wavelengths of the WSDFB

lasers without the need for additional hardware such as commercial laser wavemeter. The basis

of this mode is the optical heterodyne interference that arises when the ECDL laser wavelength

is tuned past the wavelength of a WSDFB laser. In this mode, all components shown in Figure

3.1 are used except for test section and PD2–PD8. The ECDL is tuned through 1320–1365 nm at

50 nm/s, while all WSDFB lasers are operated unmodulated (F1–F8 each set to a constant,

nonzero bias). PD1(I0) records seven interference patterns as shown in Figure 3.2b; this signal is

easily mapped to absolute wavelength using the wavelength reference method described in

Section 3.3.4. One interference pattern detailing the location of the $\lambda 2$ WSDFB laser from Figure

3.2b is shown in detail in Figure 3.2c; it can be understood as follows. When the ECDL is at

1346.9000 nm (left edge of Figure 3.2c), the beat note between the ECDL and $\lambda 2$ is at ~ 45 MHz,

too fast for the data acquisition system to resolve. As the ECDL tunes toward $\lambda 2$, the beat note

frequency decreases, and the interference becomes visible. After the ECDL tunes through $\lambda 2$, the

beat note frequency begins to increase again and ultimately disappears. The center of each

interference pattern indicates a WSDFB wavelength; each center was identified in

post-processing by an automated routine. The location of $\lambda 2$ is shown as a red dot in Figure 3.2c,

the major uncertainty identified for the wavelength axis is the MZI 2 accuracy, which

is ≥ 0.0001 cm^{-1} and < 0.001 cm^{-1} according to HITRAN2012 [22].
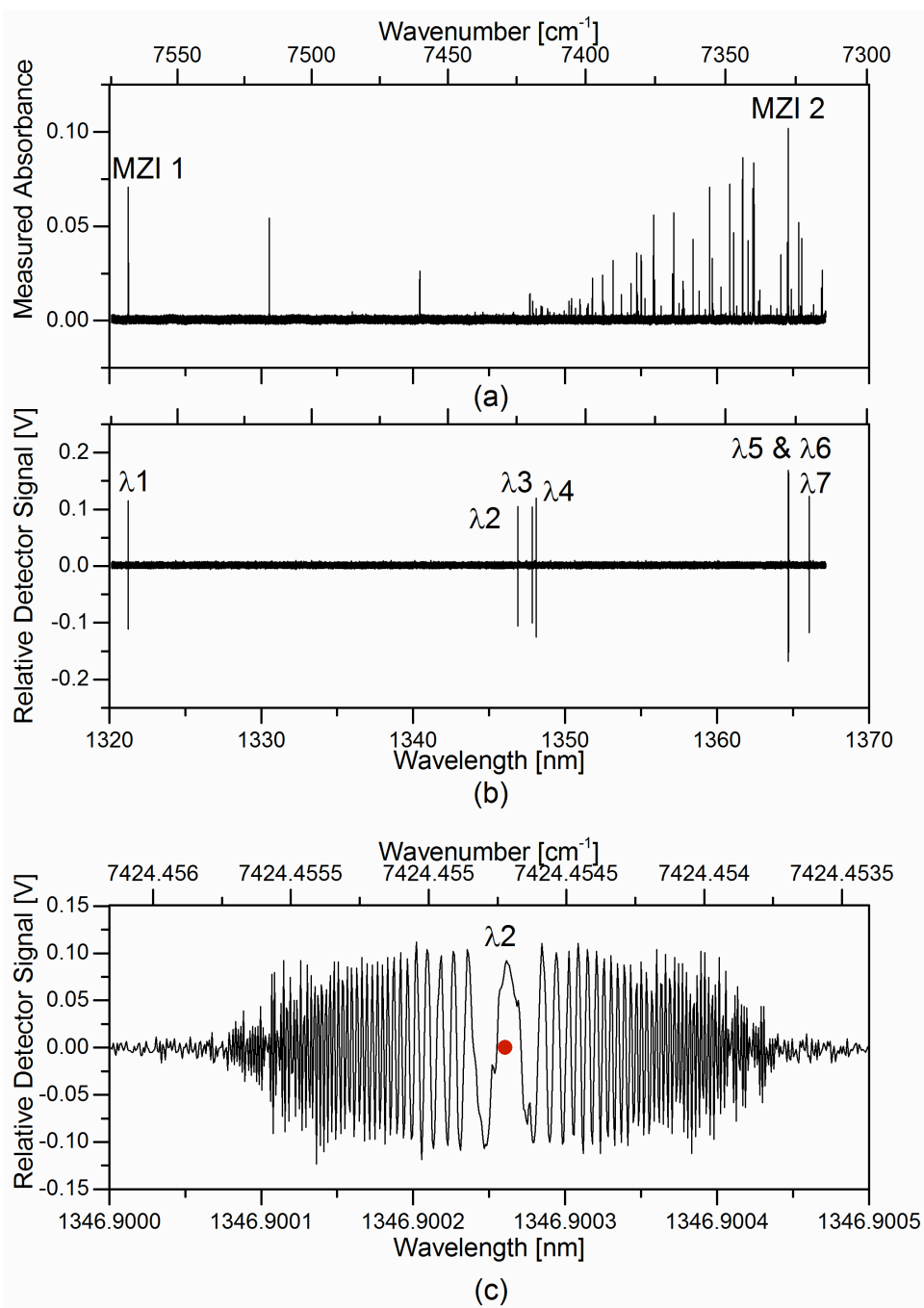
Figure 3.2 Heterodyne mode wavelength monitor traces: a) HF and H₂O series vapor cell absorption spectrum recorded using a photodiode in the reference leg, PD (Cells), b) seven heterodyne interference patterns, c) enlarged view of λ2 heterodyne interference patter

Using the ECDL as a heterodyne-based wavelength meter permits the operator to quickly and easily monitor all WSDFB lasers as needed to ensure sufficient wavelength accuracy. By contrast, commercial wavelength meters may measure only one wavelength at a time, and may be susceptible to additional errors such as an error that arises due to non-normal incidence angle of the free-space beam input to the wavemeter.

3.4.2   Spectrum-Lab

Although the main intent of the system is to use WSDFB lasers for gas temperature measurements in transient environments, the presence of the ECDL and wavelength reference leg allow for laboratory grade reference spectrum measurements as well. Such spectra are useful for understanding and improving the accuracy of FWDAS measurements. In spectrum-lab mode (see Figure 3.1), $\lambda 1$–$\lambda 7$ are not used, the ECDL is operated unmodulated (F8 set to a constant bias) and scans at 2 nm/s from 1320–1365 nm. The zero absorbance reference signal is recorded on PD1(Io), and the test section is a reference environment detected by PD2(I). Additional outputs are unused. Recorded ECDL transmission signals are first converted to absorbance using the Beer-Lambert-Bouguer law; absorption spectra are then baseline fit using a routine described by Schulze [33], to reduce wavelength-dependent baseline contamination.
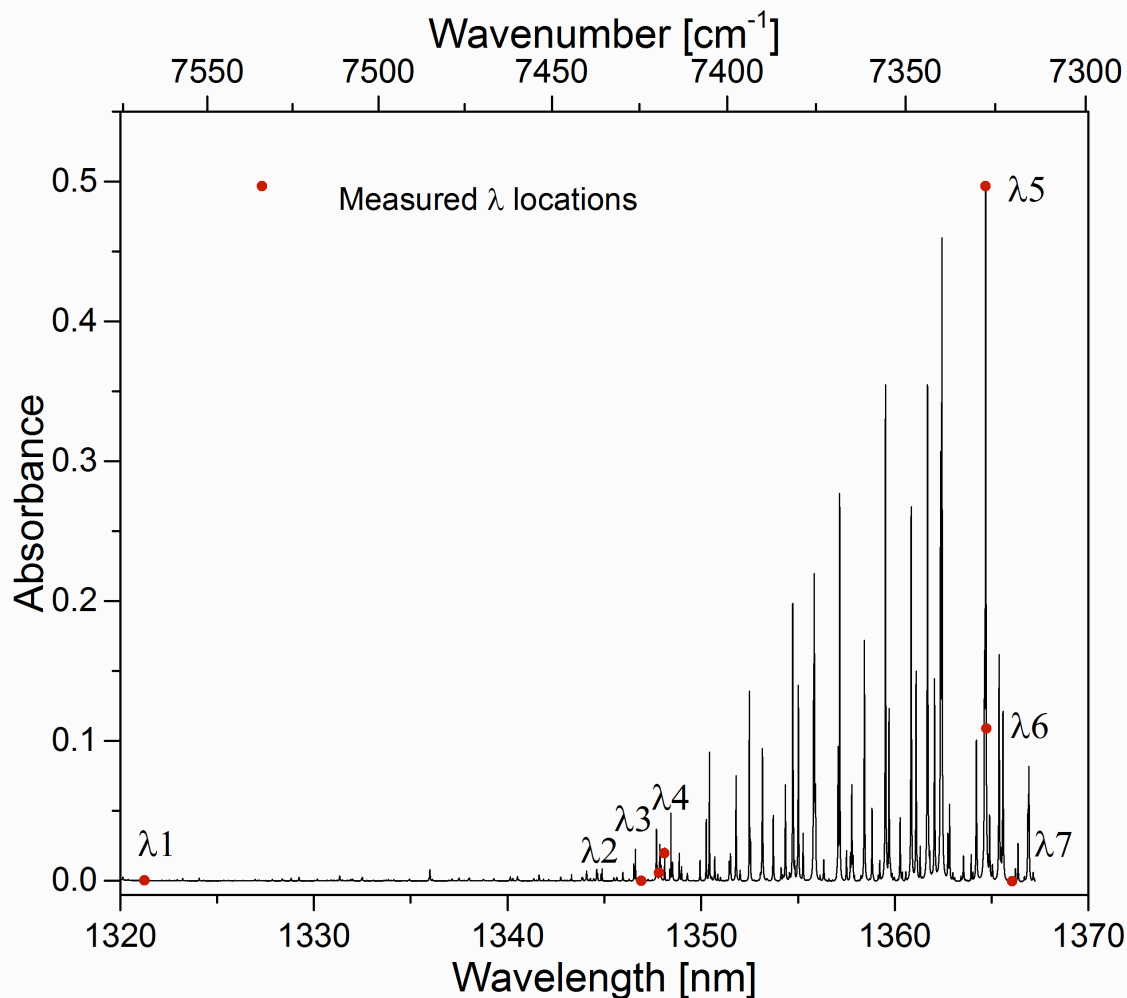
Figure 3.3 Laboratory-grade reference spectrum recorded in Spectrum-Lab mode, for gas at 1 bar and 294 K. Shown on the same plot are WSDFB laser locations in red dots, measured using Heterodyne mode.

Figure 3.3 illustrates an example result for a measurement of room air along with an overlay of the WSDFB target locations for $\lambda 5$–$\lambda 7$ as peak, near-wing, and far-wing. These are the same target locations for $\lambda 4$, $\lambda 3$, and $\lambda 2$, though it is less obvious in this room-condition case; again, all WSDFB locations were chosen for performance over temperatures from 800 K to 2100 K and pressures from 1 to 30 bar, and the near- and far-wing locations are named for their roles at elevated pressure.

3.4.3   FDM

Frequency Division Multiplex mode is the primary mode for collecting FWAS data at 7 wavelengths. In FDM mode (see Figure 3.1) all seven FWDFB lasers ($\lambda 1$–$\lambda 7$) are sinusoidally modulated (F1–F7 set to sine waves with modulation frequencies listed in Table 3.1). The multiplexed light is balanced with VOAs such that all WSDFB intensity readings are equal on PD2(I). PD2(I) is used to detect the measured signal transmitted through the test section and PD1(Io) is used to detect the zero-absorbance reference signal. The FDM signals are de-multiplexed using software-based dual-phase lock-in amplifiers at 10 kHz bandwidth. The de-multiplexed signals represent detected intensity records for each wavelength. Intensity readings are converted to measured absorbance values. Initially, these measured absorbance values have offsets with no physical relevance to the gas properties; in fact, it is common for measured absorbance values to be negative. Negative offsets can be caused by any non-ideal effect in any component optically downstream of the I and Io splitter, inclusive. For example, an uneven split ratio can lead to a negative offset. One method that can be used to correct the measured absorbance values to true absorbance values is to purge the test section with non-absorbing gas. Reference absorbance values at the purged condition are then subtracted from the measured absorbance values to yield true absorbance values. Later, during operation of the test section, true absorbance values are further corrected by subtracting the baseline wavelength $\lambda 1$ from $\lambda 2$–$\lambda 7$, and subsequently converted to temperature and mole fraction versus time as described in Section 3.2.1.

3.4.4   Spectrum-Field

Consider a practical combustion device operating at an approximately steady condition. If Spectrum-Lab mode is applied to such a device, effects such as beamsteering can overwhelm molecular transmission information such that spectrum results become unrecognizable. Methods developed by Kranendonk to reduce non-absorbing effects such as thermal emission [34] and beamsteering [35] should initially be utilized if signals are unrecognizable. However, in some cases these effects are still problematic, Spectrum-Field mode is useful in these cases.

Spectrum-Field mode uses FDM of the ECDL with one or more selected WSDFB lasers. In its simplest implementation, Spectrum-Field mode uses a single WSDFB laser ($\lambda 1$) and the scanning ECDL, tuning at 2000nm/s from 1320–1365 nm. The lasers are modulated (F1 and F8 set to sine waves with suitable modulation frequencies such as those listed in Table 3.1), and the multiplexed light is detected and de-multiplexed as described in Section 3.4.3. In contrast to Section 3.4.3, first the measured ECDL signal is divided by the measured $\lambda 1$ signal to virtually eliminate non-absorbing contamination. Recovered absorbance values are then baseline fit as described in Section 3.4.2. This technique works because the WSDFB is affected primarily by contamination, while the ECDL is affected by both contamination and molecular absorption, so that their division gives the desired molecular absorption signal. This simplest implementation effectively assumes a wavelength-flat baseline. Additional FWDFB lasers (e.g., $\lambda 2$ and $\lambda 7$, far wings) can be used to gauge the wavelength-dependence of the baseline at low pressures and allow for a subtraction that accounts for said wavelength-dependence. As shown in Figure 3.2 and described in Section 3.4.1, when the ECDL is active along with the WSDFB lasers, heterodyne pulses exist. In principle, these pulses contaminate lock in results, however the

heterodyne effect is rare enough (approximately 1 sample out of every 1 million samples) that it is generally inconsequential in this mode.

As discussed below, Spectrum-Field mode results are used in at least three unique ways: measuring temperature directly, pegging WSDFB absorbance values in devices that cannot be purged, and assessing the degree to which practical spectra match expected spectra for practical devices.

Temperature is inferred from Spectrum-Field mode results following established approaches such as those described by Kranendonk et al. [20]. In brief, measured spectra are compared with a library of simulated spectra at different temperatures and pressures until a best match is found, and the measured temperature is assigned according to this best match.

Section 3.4.3 described pegging of WSDFB absorbance values in devices that can be purged. When purging is not possible, a Spectrum-Field result can be used to peg WSDFB absorbance values as follows. After obtaining a Spectrum-Field result, pegging is performed as described in Section 3.4.3, except that instead of assigning absorbance values of zero, $\lambda1–\lambda7$ are assigned the corresponding absorbance value from the Spectrum-Field result.

Finally, one can compare a practical spectrum measured using Spectrum Field mode to the WSDFB wavelengths. Accordingly, one can check the degree to which intended WSDFB locations (e.g., peak, near-wing, and far-wing) actually correspond to those locations on the practical spectrum. For example, a wavelength intended to be located on an absorption peak shown in the database may not actually appear on a peak, owing to factors such as database errors.

3.4.5   TDM

It is straightforward to operate the system in TDM mode as opposed to FDM mode. In this mode, all eight AOMs are modulated such that they blink on and off one at a time in rapid succession (F1–F8 are set to low-duty-cycle square waves). All laser intensities are balanced by VOAs such that all intensity readings are approximately equal on PD1(Io). PD2(I) is used to detect the measured signal transmitted through the test section. This approach has been carried out previously using SOAs [10]. One benefit of TDM mode is that there is no heterodyne interference. One disadvantage is that the overall available optical power is lower, which can decrease signal-to-noise ratios.

3.5   Single channel FDM test results

Two tests were carried out in FDM mode, without aid of the ECDL, to demonstrate some aspects of the system performance. Atmospheric pressure and moderate temperature gases were used, to simplify experimental setups and to exploit the accuracy of the HITRAN2012 [22] database at ordinary conditions. Due to the fact the system is optimized for higher temperature, temperature measurements have poorer precision than would be possible with wavelengths selected for near-room-temperature conditions where tests are carried out. The first test, a dry-air purge test, is used to demonstrate temperature measurement accuracy. The second test, a steam test, qualitatively highlights the system's ability to account for optical contamination. Measured absorption data is processed according to Section 3.2.1 and Section 3.4.3: the measured absorption ratios were computed and compared to the database to infer gas temperature and mole fraction histories at 10 kHz bandwidth.

3.5.1 Dry-air purge

Optical access as described in Section 3.3.5 is constructed above a ribbon burner (Flynn HC-511) with a perforated burner surface measuring 91.4 cm x 1.9 cm. The burner is supplied with only compressed air in this non-combusting test. The total optical path length from fiber tip to photodiode is 67cm. A handheld hygrometer/thermometer (Rotronic HygroPalm21) is used to record the initial room temperature (± 0.2°C) and relative humidity (± 1%).
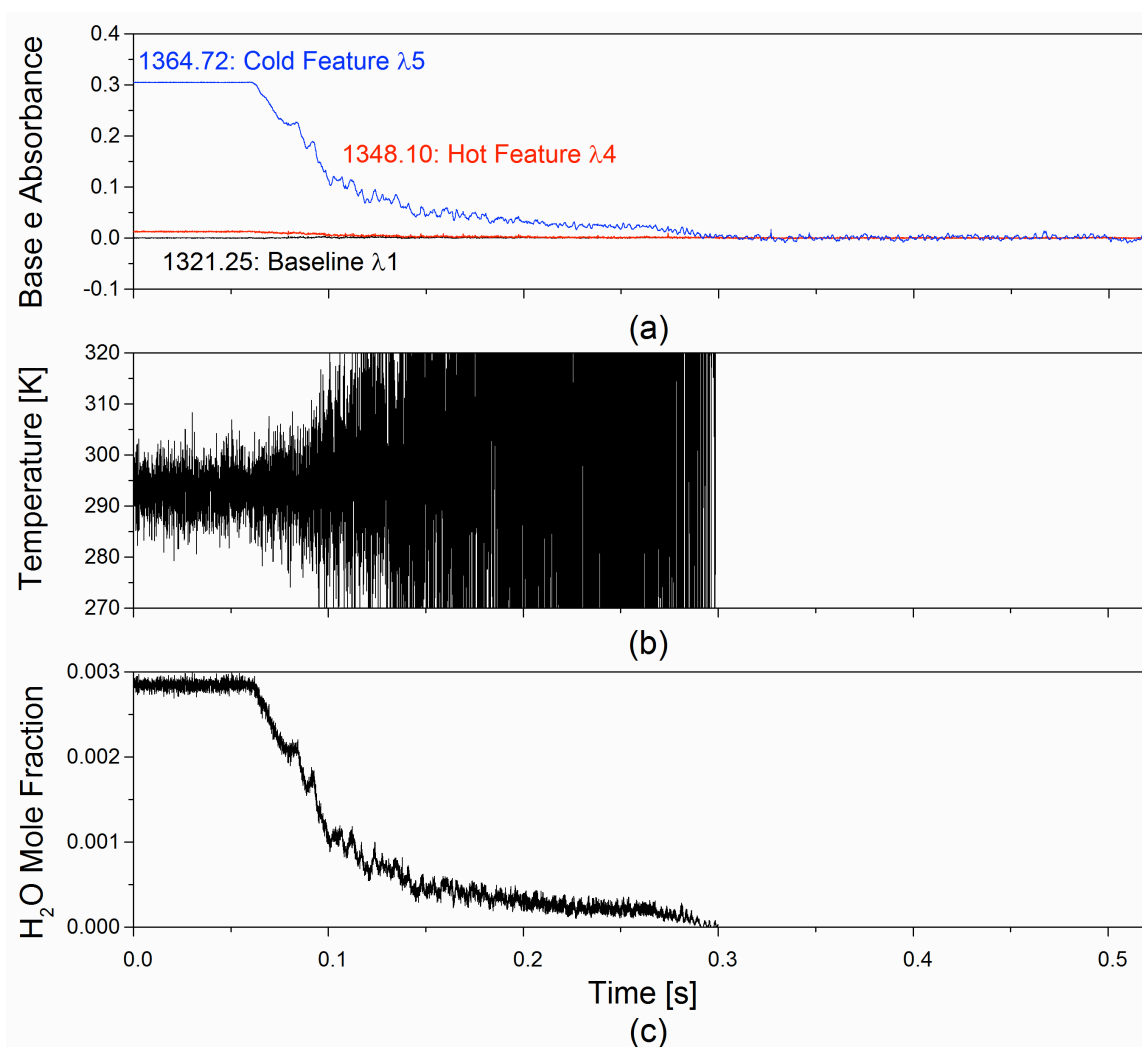
Figure 3.4 Dry-air purge test time traces: a) Relative absorbance b) Measured temperature c) Measured H₂O mole fraction

At the beginning of the test, as shown in Figure 3.4, room air is present in the beam path. The air supply valve is opened, and compressed air initiates the displacement of room water vapor from the beam path. After ~ 0.5 seconds, the beam path contains little H_2O vapor; all seven absorbance values are set to zero at this condition. Gas properties are inferred according to Section 3.2.1. During the initial time period of Figure 3.4b, $0 < t < 0.05s$, the average temperature is 292.9 K, 0.43% lower than the room temperature measured using the hygrometer/thermometer: 294.2 K. Over the same time period, the standard deviation is 3.9 K. The average H_2O vapor mole fraction found by this method, over $0 < t < 0.05s$ is 0.0028, 29.8% lower than the room mole fraction measured using a hygrometer: 0.0041. The mole fraction error is most likely caused by the lack of a true dry air reference due to humidity in the compressed air. Blank white spaces at the end of temperature and mole fraction traces in Figure 3.4b and Figure 3.4c represent areas where absorption signal levels were low, generating measurements with unacceptable signal-to-noise ratio.

3.5.2 Steam

This test demonstrates the system's ability to compensate for non-absorbing contamination. Optical access to room air as described in Section 3.3.5 is established with a path length of 60 cm. Based on hygrometer/thermometer measurements, the room air has a temperature of 294 K and a water vapor mole fraction of 0.0041. At the start of the optical test, the absorbance values are set to zero at this room condition, so that the measured absorbance values become relative to the initial room conditions. Then, after data acquisition begins, a ~2-cm-diameter steam plume produced by an electrically heated water kettle is moved into the beam path.
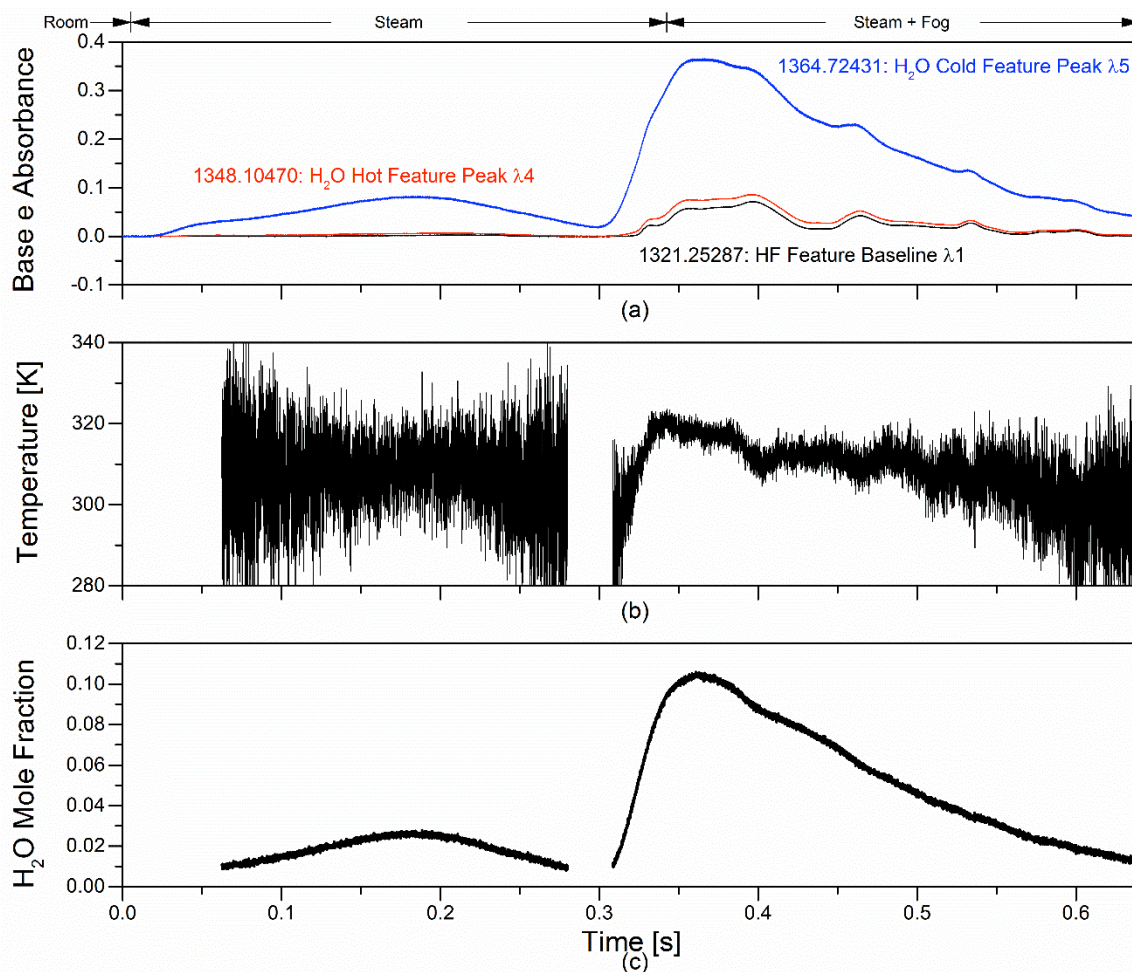
Figure 3.5 Results from the steam test, in which a ~ 2 cm-diameter steam plume is introduced into a 60-cm-long measurement beam: a) Relative absorbance b) Measured temperature c) Measured H₂O mole fraction

The data is reduced assuming the steam plume has uniform properties and a beamwise length of 2 cm. Based on this assumption, and based on zeroing absorbance values at room conditions, the results should be interpreted as semi-quantitative only; however, they still reveal interesting phenomena and sensor performance characteristics. Absorbance readings shown in Figure 3.5a clearly identify three regions: initially the room condition, second steam conditions, and finally steam plus fog conditions where the transmitted beam undergoes significant scattering by condensing water vapor. As shown in Figure 3.5a, the black trace λ1 which is essentially

unaffected by water vapor absorption suffers transmission loss of up to 7% in the steam plus fog region. This transmission loss is believed to be due primarily to scattering from fog, but minor beamsteering losses could also be present. Using simulated ratiometric values and comparing their corresponding temperatures to measured ratios, the measured temperature is inferred. Subsequently, the measured H_2O mole fraction is inferred by comparing the measured absorbance at $\lambda 5$ with the simulated absorbance at the measured temperature. In the steam region, the water vapor mole fraction peaks at ~ 0.026. At this time, the mean of the measured temperature is ~ 311 K. The corresponding relative humidity is 0.40. These conditions are consistent with the edge of the steam plume intersecting with the measurement beam. In the steam plus fog region, the water vapor mole fraction peaks at ~ 0.104, where the mean of the measured temperature is ~ 320 K. The corresponding relative humidity is 1.0, consistent with the presence of fog (identified by transmission loss at $\lambda 1$). Blank white spaces found throughout temperature and mole fraction traces Figure 3.5b and Figure 3.5c represent areas where absorption signal levels were low, generating measurements with unacceptable signal-to-noise ratios.

3.6 Conclusions

We have outlined a FWAS laser system designed for H_2O absorption thermometry over a range of temperatures and pressures (800 K to 2100 K and 1 to 30 bar). Initial tests were carried out near room temperature conditions allowing for simple experimental setups and exploiting the accuracy of the HITRAN2012 [22] database at these conditions. The future of this system relies heavily on the continued improvement of spectral databases, specifically at combustion conditions. While primarily a fixed-wavelength system, an on-board ECDL enables multiple modes that enhance FWAS measurement accuracy and the capability to reduce contamination in spectral scans. The heterodyne mode assists in accurate wavelength identification. The present system can be used for improving spectral databases, because spectrum-lab mode can be used to obtain high-quality reference spectra in gas samples at known temperatures and pressures. Our continued use of this system to further enrich reference databases along with others such as Rieker et. al. [19] will allow for efficient temperature measurements in practical environments.

Chapter 4. H₂O absorption cross-section database development

4.1 Motivation

H_2O absorption spectroscopy in the 1320 - 1380 nm range is used extensively for combustion sensing and diagnostics. H_2O absorption thermometry requires the ability to match measured spectra[26], or set of discrete absorbance values, to spectra that have either been simulated using a molecular spectral database or to spectra that have been previously measured at known conditions. At high temperatures $(1000 - 2100 \text{ K})$, the leading spectral databases (HITEMP2010 [23] and BT2 [36]) are woefully inadequate for simulation of H_2O absorption spectra for use with thermometry throughout the $0.5 - 50$ bar range. For example, BT2 contains no broadening data, and the broadening data in HITEMP2010 is so inaccurate that researchers will commonly replace thousands of line-by-line broadening coefficients with a single generalized value to achieve better performance. In addition, the use of traditional lineshape profiles such as Gaussian, Lorentzian, Voigt, Rautian, and Galatry, have been shown by Goldenstien [28] and others to result in errors when used to compute H_2O spectra over a range of conditions. Significant effort has recently been made by others to identify lineshape functions that accurately depict H_2O-, CO_2-, & N_2-perturbed H_2O spectra. A recent IUPAC technical report [37] recommends the use of the Hartmann-Tran profile (HTP) as the universal model for simulation of spectral lines in the gas phase. Although a lineshape model has been chosen, few lineshape parameters have been simulated or measured for species of interest at combustion conditions. The most advanced spectral lineshape model that can be computed using HITEMP2010 is the Voigt profile, and even then only binary compositions are accounted for through H_2O-H_2O and H_2O-Air collisional broadening. Unfortunately, traditional molecular

databases become increasingly deficient the further one gets from the atmospheric conditions for which they were initially developed. Errors in transition parameters such as position, strength, lower-state energy, pressure shift coefficient and their temperature exponent, and broadening coefficient and its temperature exponent create challenges for full-spectrum spectroscopy. For example,

Figure 4.1 shows residuals over 20% when a HITEMP2010 simulation is compared to an ECDL furnace measurement at 1723 K, 0.943 bar and 3.8% H_2O.
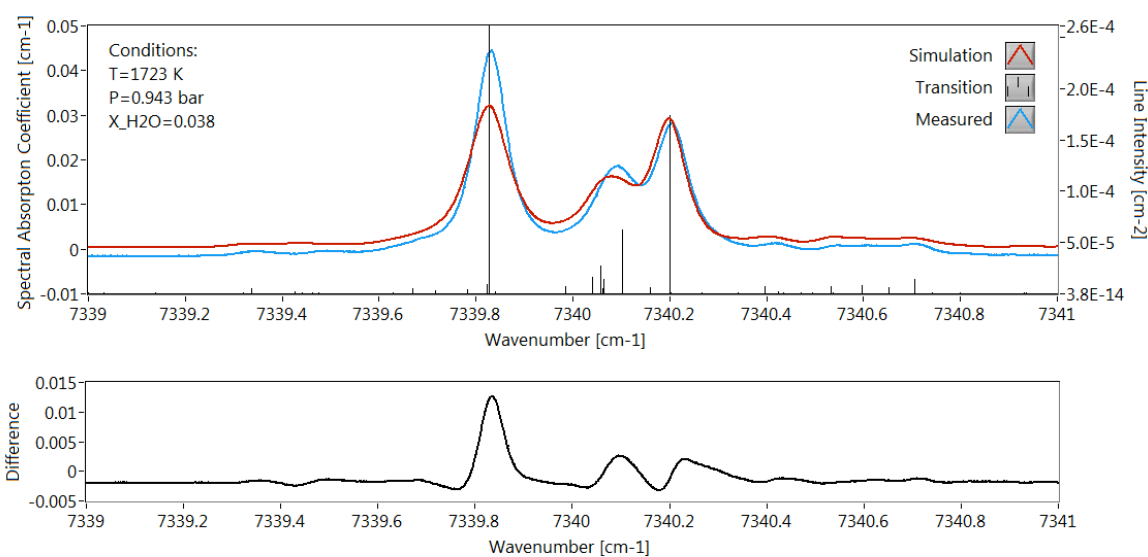
Figure 4.1 Top, measured and simulated 3.8% H_2O spectra at 1723 K and 0.943 bar. Bottom, absorbance difference between simulation and measured.

Errors are especially problematic in FWAS due to increased reliance on the absolute accuracy of the relevant spectral locations. The molecular databases must be updated before the full realization of absorption thermometry can be achieved. By investigating the different approaches to database architecture, we look to gain an advantage in the ability to make thermometry measurements at combustion conditions.

4.2   Background: Line-by-line versus cross-section databases

A principle concept relevant to this thesis is the distinction between line-by-line and absorption cross-section databases. Consider an isolated absorption transition illustrated by the blue vertical line in Figure 4.2A. Only considering the traditional Voigt lineshape, and assuming a collisional environment of H_2O, CO_2, and N_2, 15 total parameters are required. Specifically, there are 3 transition parameters (line position ν [cm^{-1}], line strength S [cm^{-2}-atm^{-1}], lower-state energy E" [cm^{-1}]), and 12 lineshape parameters for each transition. The 12 lineshape parameters are 3 broadening coefficients γ_{abs-N2}, $\gamma_{abs-H2O}$, $\gamma_{abs-CO2}$, their associated temperature exponents $n_{\gamma N2}$, $n_{\gamma H2O}$, $n_{\gamma CO2}$, and 3 pressure shift coefficients δ_{abs-N2}, $\delta_{abs-H2O}$, $\delta_{abs-CO2}$, and their associated temperature exponents $n_{\delta N2}$, $n_{\delta H2O}$, $n_{\delta CO2}$. The Voigt lineshape commonly breaks down because effects such as Dicke narrowing and / or speed-dependent broadening become important, requiring additional lineshape parameters, but we will ignore such effects in this section.
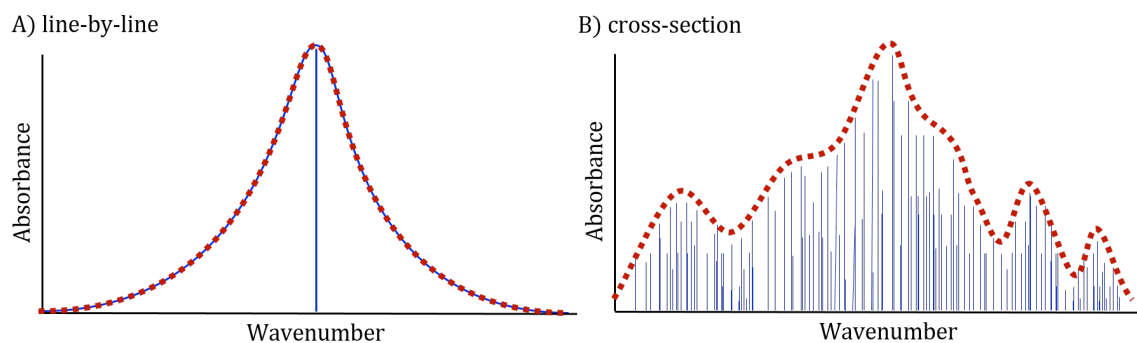
Figure 4.2 Illustration of a case (A) where a line-by-line database is more appropriate, and (B) where a cross-section approach is more appropriate. Red squares indicate measurement points and blue lines are the actual spectra.

Accordingly, given the 15 parameters, one can accurately model the absorption feature at any condition, as shown by the thin blue curve in Figure 4.2A. To obtain the 15 parameters from experiments, one would measure data as shown by the red squares in Figure 4.2A for various

conditions. Each dataset of red squares would contain typically 1000 data points, and the minimum total number of conditions tested typically would be 9. So, with 1000 x 9 = 9000 data points, one could infer the 15 parameters and would then be capable to model the spectrum for this single isolated absorption transition at any arbitrary conditions. This is a worthy arrangement, compared to the cross-section approach for this same case. In the cross-section approach, one would ignore the transition parameters and instead measure the 1000 data points for typically 86,400 conditions to develop an interpolation-friendly empirical database of measured spectra. Since 1000 x 86,400 = 86.4 million is much greater than 9000, the line-by-line approach is at a clear advantage.

In comparison, reconsider a congested group of 1 million absorption transitions as illustrated in Figure 4.2B. In this case, the LBL approach is after 15 parameters x 1 million transitions = 15 million parameters. One might attempt to infer these 15 million parameters from 1k data points over 9 conditions = 9000 data points again, but find this is intractable for multiple reasons, perhaps the most obvious being the undetermined mathematical system (9000 equations in 15 million unknowns). Furthermore, the 86.4 million data points are relatively simple to store and process compared to 15 million parameters: if one needs 15 million parameters to specify the spectrum, one might just as well store the 86.4 million data points worth of raw spectra. The case shown in Figure 4.2A is typical of small molecules such as di-atomics, or tri-atomics at room temperature. It is the basis for line-by-line databases such as HITEMP2010 [23]. The case shown in Figure 4.2B is typical of large molecules such as n-heptane, or smaller molecules at high temperature like H_2O. It is the basis for absorption cross-section databases such as the catalogs of Fourier-transform infrared (FTIR) data available from Pacific Northwest National Laboratory (PNNL) [38].

4.3 Line-by-line approach

Traditional high-temperature molecular databases such as HITEMP2010 [23] present absorbance spectra in a line-by-line (LBL) format consisting of a set of parameters that describe the transition and its lineshape as shown in Equation 4.1. Here the absorbance, $\alpha(v)$, is a function of wavenumber, and is expressed as the sum over all absorption transitions denoted as j.

$$\alpha(v) = \sum_{j} S_j(T) P \chi_{abs} \varphi_j(v, T, P, \chi) L$$

Equation 4.1 Absorbance in a line-by-line form

$S(T)$ $[cm^{-2}atm^{-1}]$ is the line strength as a function of temperature, P [atm] is the gas pressure, T [K] is the gas temperature, χ is species mole fraction, φ [cm] is the lineshape function, L [cm] is the path length, and v $[cm^{-1}]$ is the wavenumber. The LBL approach is founded on the ability to extract or compute the transition and lineshape parameters, along with their composition, temperature and pressure dependence, for all significant transitions. A significant transition, for this discussion, is defined as a transition yielding an absorbance that is less than the anticipated absorbance noise level of 1×10^{-4}. A major advantage of the LBL approach is that it only requires an absolute minimum four measured spectra per collisional species. These four spectra (labeled $1 - 4$ in Figure 4.3) are measured at the composition of 0.1% H_2O to 99.9% N_2, to represent a case with primary N_2 broadening, as shown in Figure 4.3. The spectra are measured at: the maximum temperature obtainable in a reference cell at a low pressure (spectrum 1) so collisional effects are negligible, the maximum temperature and a slightly higher pressure (spectrum 2) to capture collisional effects, a slightly lower temperature at a low pressure (spectrum 3) to capture lower-state energy, and the same temperature as spectrum 3 at a slightly higher pressure (spectrum 4) to capture temperature-dependence of collisional effects. Using

these measured spectra along with physics-based models to extract lineshape parameters, one can extrapolate over the entire HTPD range of interest, dramatically reducing the necessary recorded spectra relative to the σ_{abs} approach.
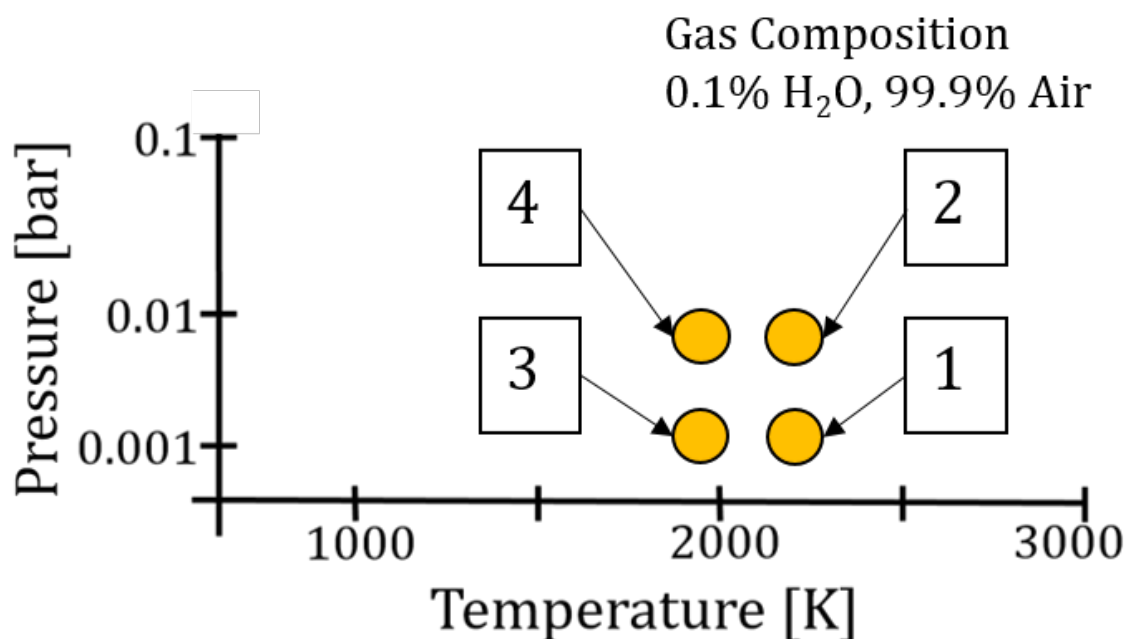
Figure 4.3 LBL spectra measurement conditions denoting spectra measurements points 1, 2, 3, and 4.

4.3.1 Model study of single isolated transition

In order to assess feasibility of the LBL approach, a test was performed to determine the minimum absorbance from which parameters can still be reliably extracted. A single Gaussian line was simulated with a full-width half-max (FWHM) of 0.058 cm^{-1}. Gaussian white noise (GWN) with a standard deviation of 1 x 10^{-4}, typical of ECDL measurements, was added to the simulation. Using a differential-evolution genetic algorithm (DE-GA), a fit was performed 1000 times, each time using a fresh realization of GWN. An example of one fit is shown in Figure 4.4. From this fitting routine, it was found that a transition with an absorbance peak of 5 x 10^{-4} could be resolved with an acceptable root mean square (RMS) peak absorbance error = 0.99%. A peak

absorbance of 5×10^{-4} corresponds to a transition with a line strength, S, of 2×10^{-24} cm^{-2}-atm^{-1}. This is the minimal strength of a single isolated transition that can be successfully recovered with a RMS peak absorbance error $\leq 1\%$.
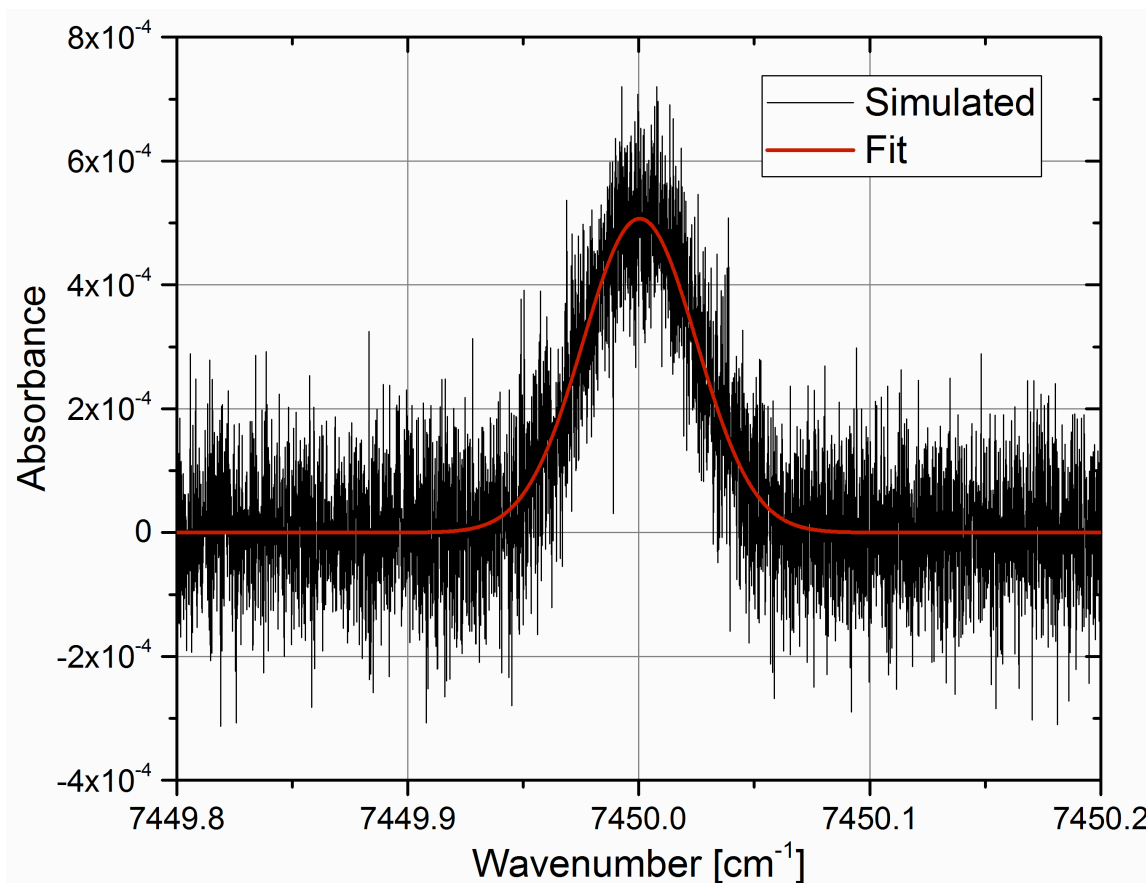
Figure 4.4 Single Gaussian line simulated with a 5×10^{-5} absorbance peak and Gaussian white noise standard deviation of 1×10^{-4}, is shown in black. The DE-GA fit with a RMS peak absorbance error < %1 is shown in red

The minimal recoverable line strength is used as a cutoff strength for all transitions in the 7300 - 7600 cm^{-1} range. First, a complete 2123 K spectrum is simulated using a Gaussian lineshape with a FWHM = 0.058 cm^{-1} for all transitions in the range. Second, the simulation is repeated, this time retaining only transitions with line strengths greater than 2×10^{-24} cm^{-2}-atm^{-1}.

Using this cutoff strength leaves only 3504 transitions in the range. The difference between the two spectra is taken as the residual, which is presented in Figure 4.5.
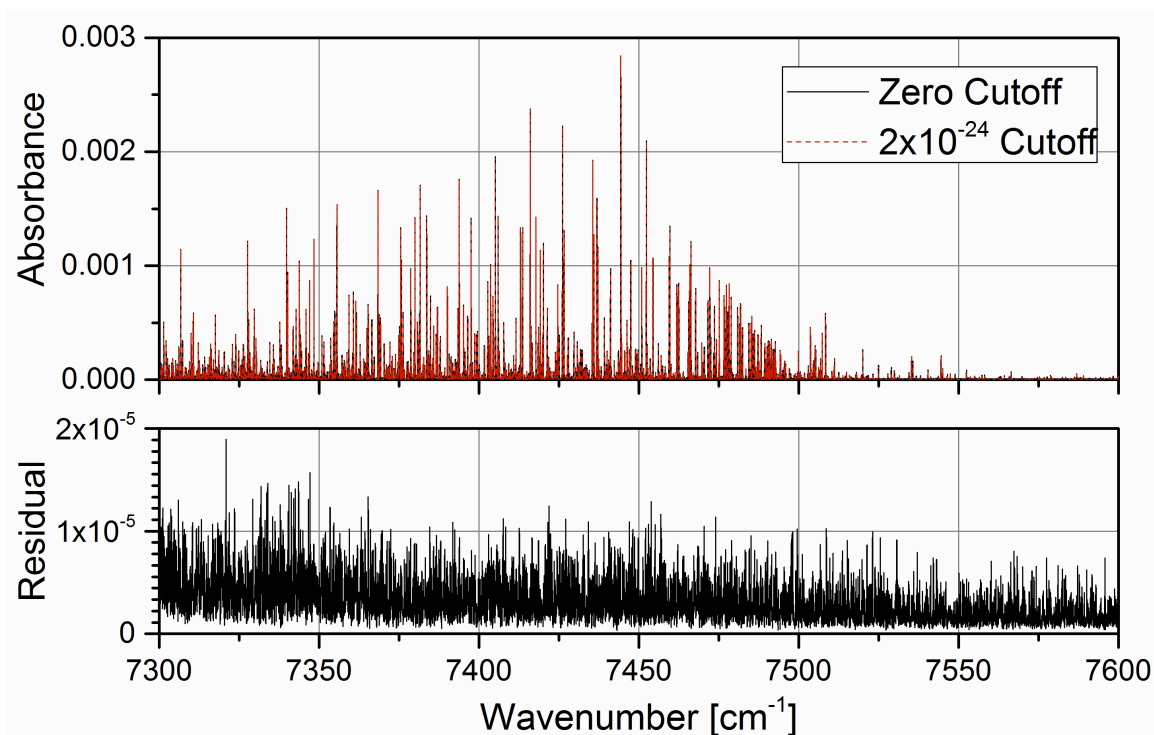
Figure 4.5 Top, H$_2$O absorption spectra simulated by HITEMP2010, Gaussian lineshape, and at 2123 K with different minimum transition strength cutoffs. Solid black, no transitions removed; dashed red, transitions with strength S < 2 x 10^{-24} cm^{-2}-atm^{-1} are removed. Bottom, residual of H$_2$O absorbance spectra when 2 x 10^{-24} cutoff is used.

We divide the maximum absorbance of the spectrum simulated with the line strength cutoff by the maximum absorbance of the residual to obtain a quantity we call the signal-to-residual ratio (SRR), as shown in Equation 4.2.

$$SRR \equiv \frac{Max\ Absorbance\ Signal}{Max\ Absorbance\ Residual}$$

Equation 4.2 Signal-to-residual ratio

At 2123 K, the SRR based on the than 2×10^{-24} cm^{-2}-atm^{-1} cutoff is 1.5×10^2. Most researchers are looking for max absorption errors of reference spectra to be less than 0.01% for results to be acceptable. Based on experience we set the absorption error to 0.01% as our target. This 0.01% absorbance error corresponds to a SRR $= 1 \times 10^4$.

This assessment suggests that, in the hypothetical and ideal case where all transitions are isolated, the SRR would still be unacceptable.

4.3.2   Model study of two transitions in close proximity

At high temperatures and in the 7300 - 7600 cm^{-1} range, there are few if any transitions that are well isolated.   We expect that congestion will ultimately reduce the corresponding SRR to a value below 1.5×10^2 for our test case. To begin to understand the effects of congestion on SRR, we evaluated the ability to extract lineshape parameters in the case of two transitions in close proximity.   The DE-GA is again used to fit two simulated Gaussian lines with FWHM $= 0.058$ cm^{-1}, as shown in Figure 4.6. Again, GWN with a standard deviation of 1×10^{-4} is added. Here, the green transition, Fit A, is fixed in line position (7450 cm^{-1}) and peak absorbance of 0.08. The blue transition, Fit B, is varied in peak absorbance, H, and wavenumber separation, Δv [cm^{-1}]. The red dashed line, Fit A+B represents the sum of Fit A and Fit B. The fit was performed 50 times, using unique GWN each time, and the RMS peak absorbance error is computed between the Fit A+B and the sum of two simulated lines with added GWN, shown black.
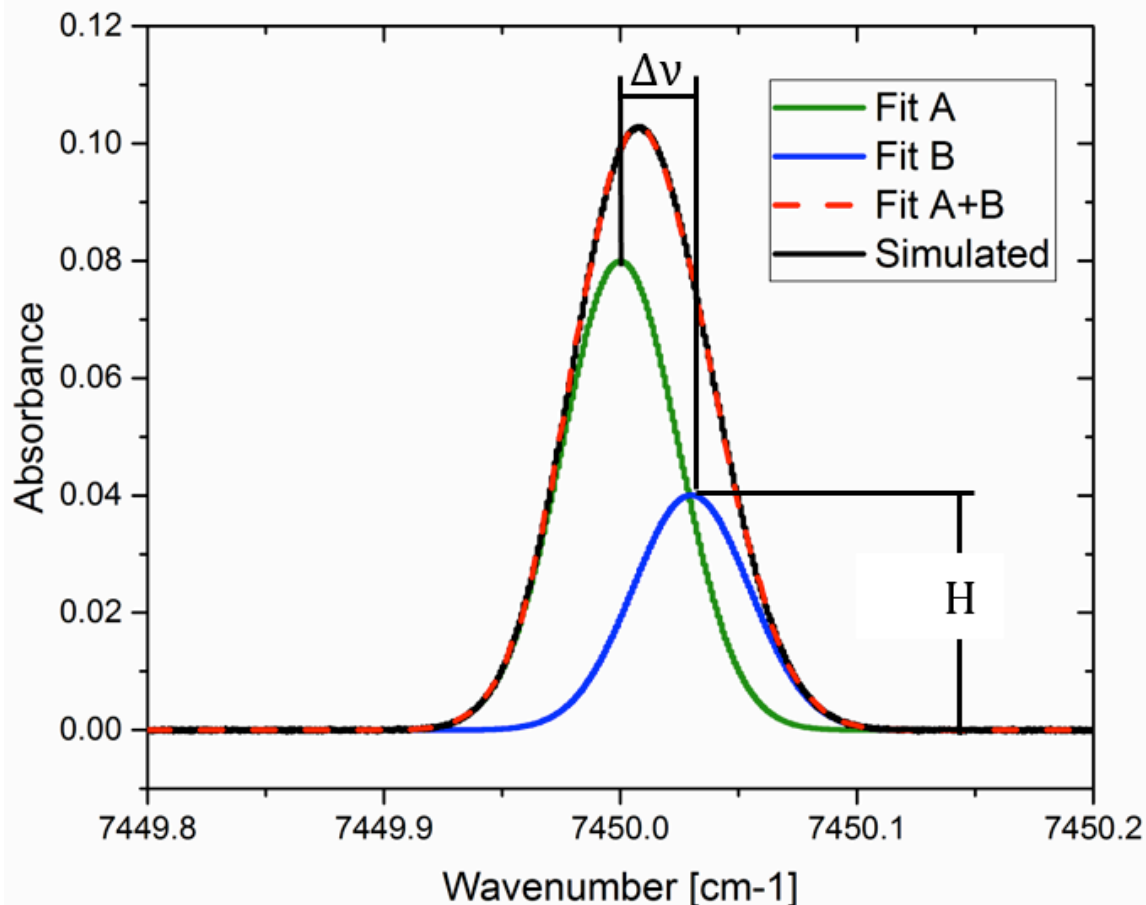
Figure 4.6 Two Gaussian line DE-GA fit example. The green line, Fit A, is fixed in line position (7450 cm^{-1}) and peak absorbance of 0.08. The blue line, Fit B, is varied in peak absorbance, H and peak wavenumber separation, Δv [cm^{-1}]. The red dashed line, Fit A+B represents the sum of Fit A and Fit B. The error is computed between the Fit A+B and the simulated lines with added GWN, shown black. The GWN has a standard deviation of 1 x 10^{-4} and all Lines have a FWHM = 0.058 cm^{-1}.

The results from these DE-GA fits are presented in Figure 4.7. The red dot represents an example case with a separation distance $\Delta v = 0.0147$ cm^{-1}, and Fit B peak absorbance of 0.0344 (43% of Fit A's peak absorbance). All combinations of H and Δv in the shaded region have a RMS absorbance peak error > 1%; therefore, the shaded region is the undesirable region. The plot shows that in cases of a weak peak in close proximity to a strong peak (H= 0.08), it is difficult to reliably extract parameters for the weaker peak (Fit B).
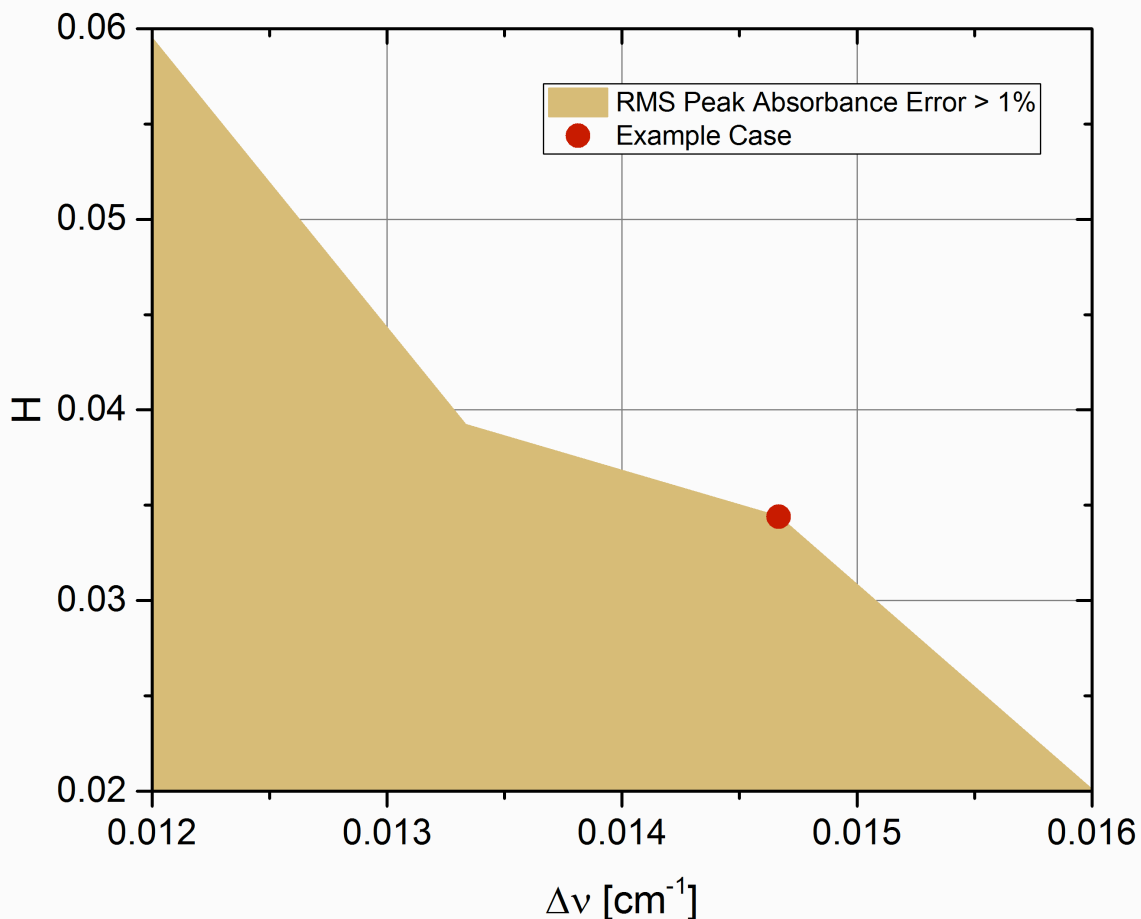
Figure 4.7 Results from fitting two Gaussian lines with varied peak separation distance, Δν, and peak absorbance, H, for the weak transition, Fit B in Figure 4.6. The red dot represents an example case with a separation distance Δν = 0.0147cm^{-1}, and peak absorbance H = 0.0344.

Looking further into the example case highlighted by the red dot, we ran a simulation to estimate the prevalence of such levels of congestion. We tested the strongest 3500 transitions at 2123 K, representing the 3504 transitions that are found resolvable in the 1 line model study in Section 4.3.1. About each transition a window of half-width 0.0147 cm^{-1} is centered. The strengths of the other transitions in the window are considered relative to the 43% value described above. Representative results are shown in Figure 4.8.
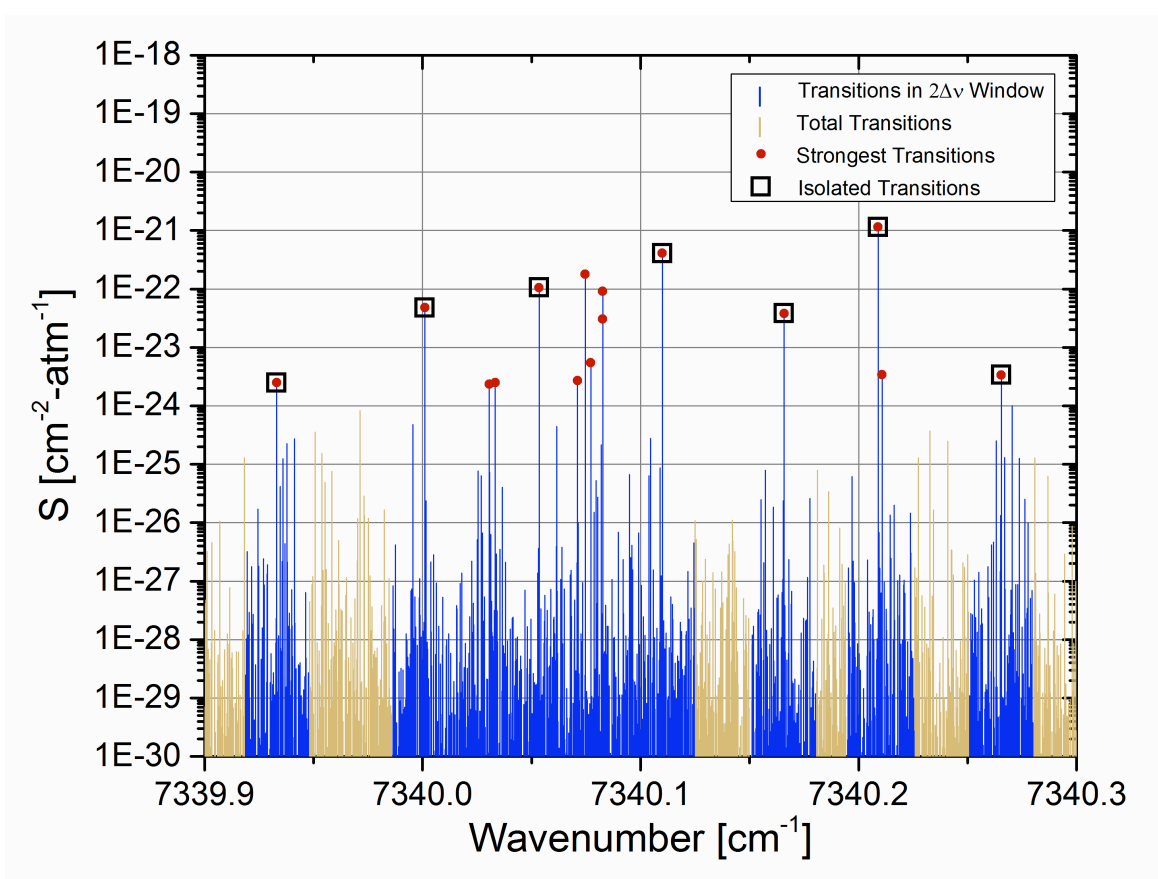
Figure 4.8 Example showing isolated transitions. All transitions in the limited spectral range shown appear in tan. Transitions that belong to the set of the strongest 3500 are shown with red dots. Blue lines represent transitions in 0.0147cm^{-1} halfwidth windows centered on the strongest 3500 transitions. Isolated transitions are shown by a black box. In this example there are 15 strong transitions but only 7 are isolated.

A small wavelength range is shown for clarity. All transitions in the HITEMP2010 database in this range are displayed in tan. Transitions that belong to the set of the strongest 3500 transitions in the 7300-7600 cm^{-1} range are indicated by red dots. Transitions inside the $2\Delta v$ windows that are centered on strongest transitions are presented in blue. Isolated transitions were identified as transitions belonging to the set of the 3500 strongest transitions that also have no other transitions in the windowed range with strength greater than 43% of the transition's strength. By this definition, only 70.7% of the 3500 transitions are isolated. Therefore, transition congestion effectively reduces the single isolated transition SRR value of $\approx 1.5 \times 10^2$, found in Section 4.3.1,

to a significantly lower value. The actual value has not been determined. These results suggest the LBL approach is unable to sufficiently produce reference spectra with a SRR greater than 1×10^4.

4.4 Absorption cross-section approach

Herein, absorption cross-section (σ_{abs}) approach refers to the architecture of an empirical spectral database created by collecting spectra at numerous conditions using an automated variable-temperature, -pressure, and -composition gas cell. The absorbance spectra is represented in a cross-section format that differs from Equation 4.1, due to the fact that parameters are no longer on a per transition basis, as shown in Equation 4.3,

$$\alpha(\nu) = n\chi_{abs}\sigma_{abs}(\nu, T, P, \chi)L$$

Equation 4.3 Absorbance in cross-section form

where, n [molecules-cm^{-3}] is the number density of the gas and σ_{abs} [cm^2 -molecule^{-1}] is the absorption cross-section of the absorbing species. The σ_{abs} approach environmental test conditions cover a range of temperatures (1000 K < T < 2100 K), pressures (0.5 bar < P < 50 bar), and molar composition (0.01 < X_{H2O} < 0.2, 0.0 < X_{CO2} < 0.2, in a N_2 buffer). The gas mixtures chosen should span the range of anticipated combustion product mixtures. Mixtures would be formulated from different amounts of H_2O, CO_2, and N_2. For example, Figure 4.3, represents the gas composition of 1% H_2O and 99% N_2, which effectively characterizes N_2 broadening of H_2O. In order to recover σ_{abs} spectra at conditions not found explicitly in the database one must interpolate. The interpolation is evaluated in three parts, first σ_{abs} spectra are interpolated as a function of pressure, then temperature, and finally σ_{abs} spectra are interpolated as a function of H_2O and CO_2 molar compositions.

4.4.1 $\sigma_{abs}(P_{user})$ interpolation study

An initial test evaluated the ability to interpolate absorbance spectra over a range of pressures. Spectra of varying pressures, $0.5 < P < 50$ bar, were simulated over the 7450-7475 cm^{-1} range using the HITEMP2010 [23] database and a Voigt lineshape with a fixed temperature $T = 2120$ K, spectral resolution of 0.0001 cm^{-1}, path length $L = 152.4$ cm, and water mole fraction $X_{H2O} = 0.01$.

Linear and logarithmic pressure spacing were found to underperform, so a hybrid pressure spacing function was used, shown in Equation 4.4,

$$P_{i+1} = f * P_i + \Delta P$$

Equation 4.4 Hybrid pressure spacing function

where, P_i [bar] is the initial pressure, P_{i+1} [bar] is the subsequent pressure, f is the multiplicative pressure factor, ΔP [bar] is the pressure increment. A pressure range of $0.5 - 50$ bar with $f = 0.02$ and $\Delta P = 0.2$ bar results in 89 pressure steps. An additional measurement ($P \sim 0$) is required for baseline reference, resulting in a total of 90 pressure steps. A database of simulated absorbance spectra is created using HITEMP2010 [23], and a 1D spline is used to interpolate absorbances over all pressure conditions. Figure 4.9 represents an example of the absorbance signals of the interpolated(top, solid black) and simulated reference(top, dashed red) along with the residual(bottom), corresponding to the pressure interpolated σ_{abs}(red dot) as shown in Figure 4.10. This example has a SRR $= 1.23$ x 10^4, and the σ_{abs} was interpolated as $P = 16.37$ bar between database σ_{abs}'s with pressures of 16.109 bar and 16.632 bar. All interpolated spectra at each pressure have a SSR computed in the same manner as Equation 2.1.
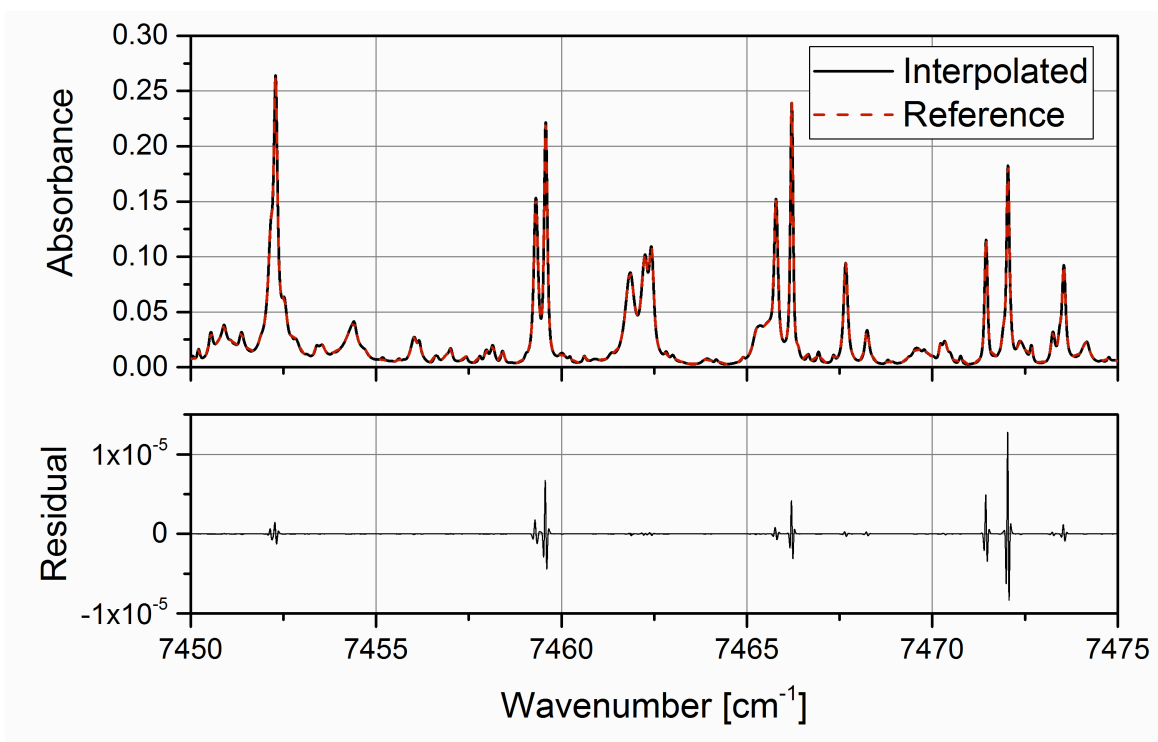
Figure 4.9 Pressure interpolation study. Top simulated reference spectra, red dash, compared to interpolated spectra, solid black. Bottom residual for spectra with T = 2120 K P = 16.37 bar, and X_{H2O} = 0.01.
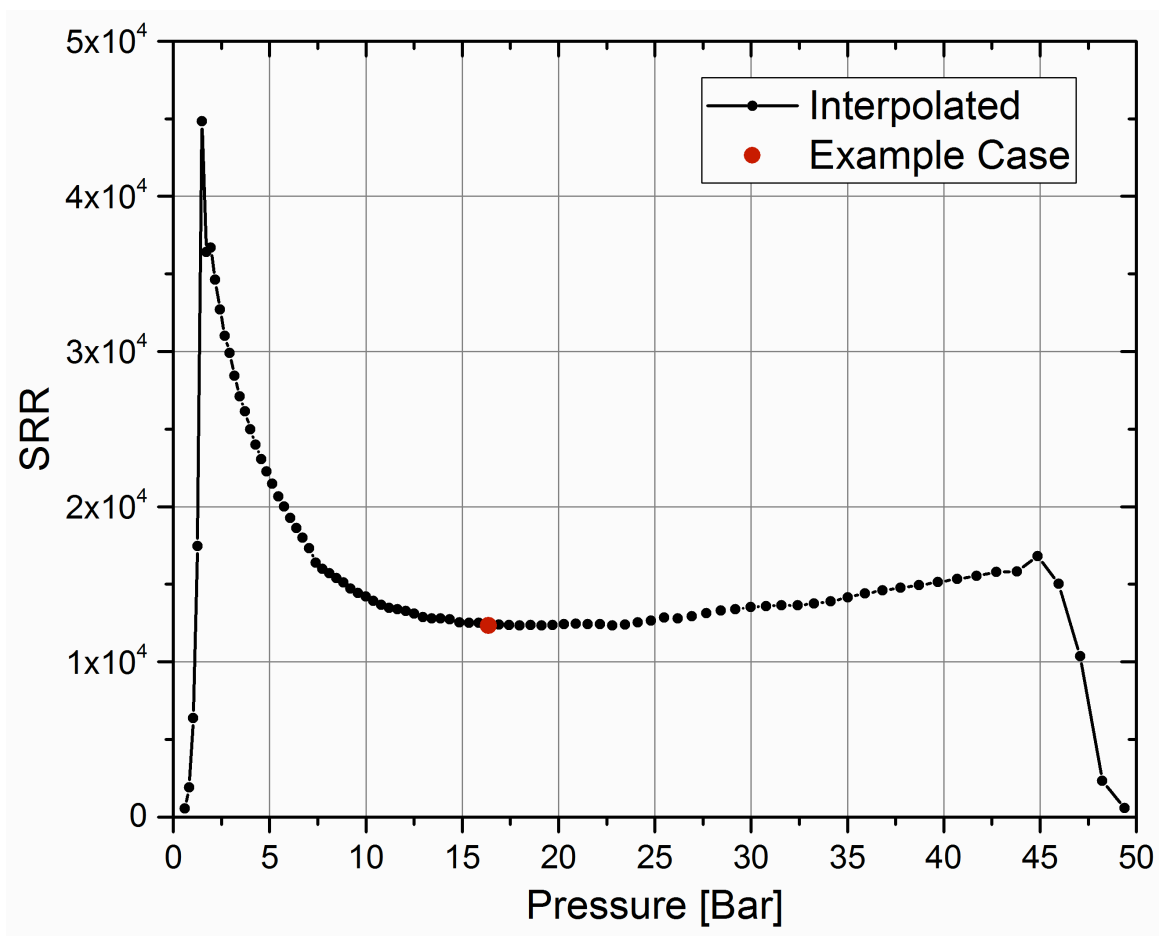
Figure 4.10 SRR for interpolated σ_{abs} with varied pressure. Example Case represents a SRR = 1.23 x 10^4, T = 2120 K, P = 16.37 bar, and X_{H2O} = 0.01.

Some performance is lost near the edges of the pressure database. This attributed to the end conditions of the spline interpolation, which do not use a fixed end condition. Excluding the edges, the interpolation successfully returns a SRR >1 x 10^4. A more sophisticated pressure spacing function could be used to further optimize the spacing to decrease the number of pressures required.

4.4.2 $\sigma_{abs}(T_{user})$ interpolation study

In a similar way, we evaluated temperature interpolation. Spectra of varying temperatures, $1000 < T < 2100$ K, were simulated over the 7450-7475 cm^{-1} range using the HITEMP2010 [23] database, the Tennyson Vidler partition function [39], and a Voigt lineshape with a fixed pressure $P = 0.5$ bar, spectral resolution of 0.0001 cm^{-1}, path length $L = 152.4$ cm, and water mole fraction $X_{H2O} = 0.01$. The Tennyson Vidler partition function was chosen for improved smoothness relative to the standard total internal partition sums (TIPS) [40]. A linear temperature spacing function was chosen using 15 temperatures. Using this spacing, a database of absorbance spectra is created, and a 1D spline is used to interpolate absorbances over all temperature conditions. Figure 4.11 represents an example of the absorbance signals of the interpolated (top, solid black) and simulated reference (top, dashed red) along with the residual (bottom), corresponding to the pressure interpolated σ_{abs} (red dot) as shown in Figure 4.12. This example has a SRR = 1.48 x 10^4, and the σ_{abs} was interpolated as $T = 1189.66$ K between database σ_{abs}'s with temperatures of 1151.72 K and 1227.59 K. All interpolated spectra at each pressure have a SSR computed in the same manner as Equation 2.1.
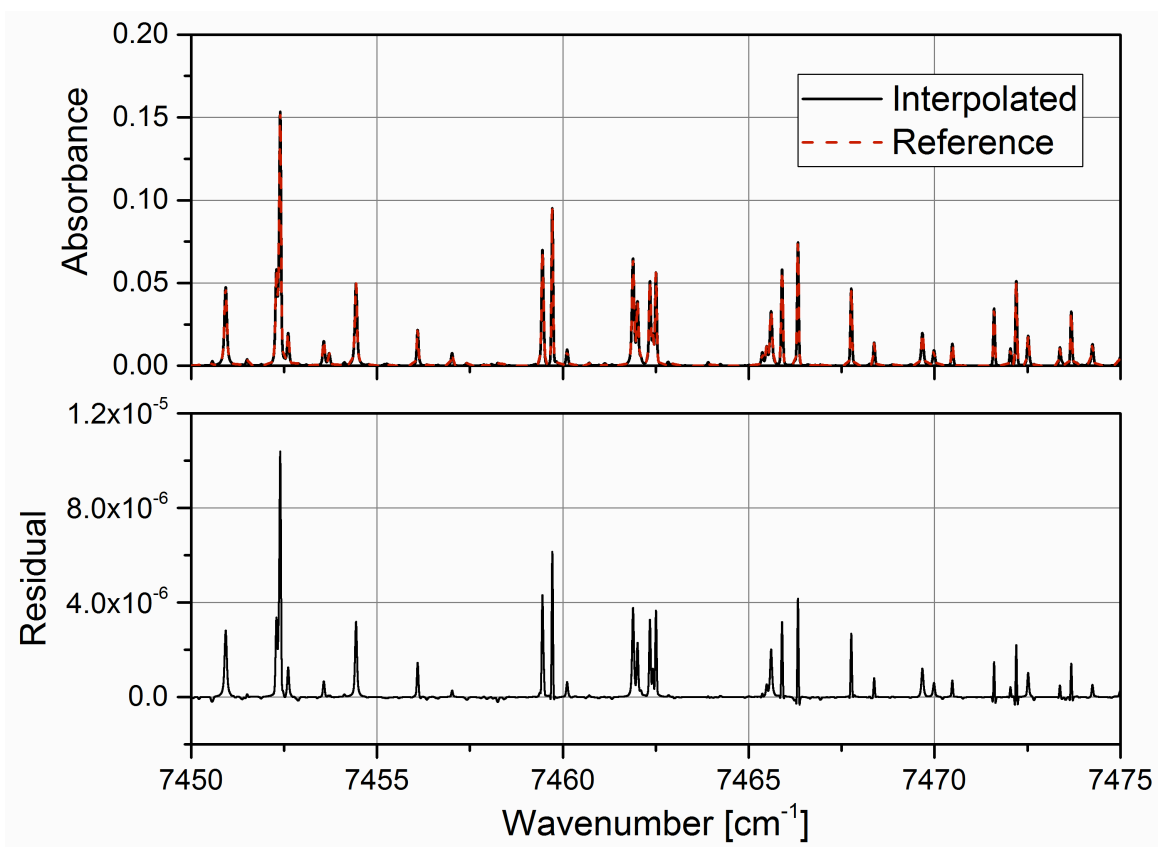
Figure 4.11 Temperature interpolation study. Top shows simulated reference spectra, red dash, compared to interpolated spectra, solid black. Bottom shows residual for spectra with T = 1189.66 K, P = 0.5 bar, and $X_{H2O} = 0.01$.
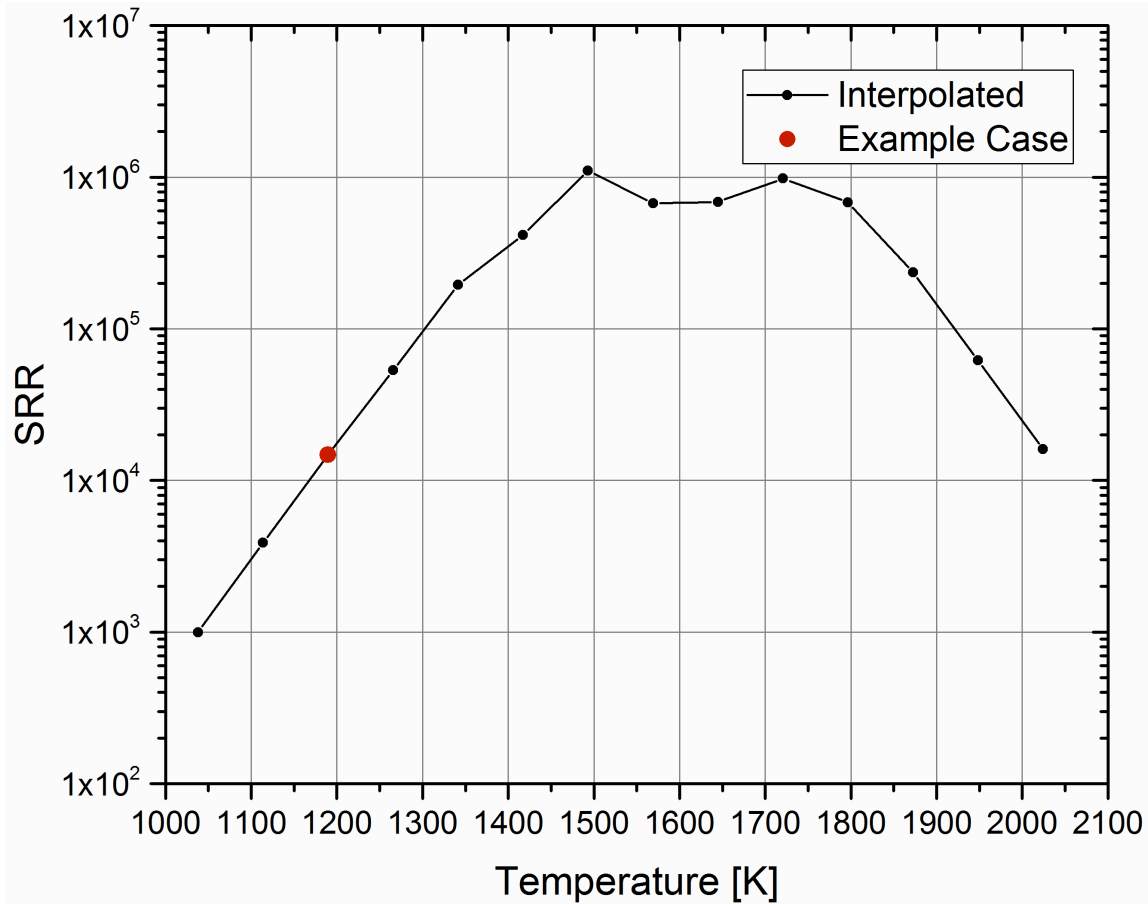
Figure 4.12 SRR for interpolated σ_{abs} with varied temperature. Example Case represents a SRR = 1.48 x 10^4 and T = 1189.66 K, P = 0.5 bar, and X_{H2O} = 0.01.

Once again using the spline interpolation some performance is lost near the left edge of the temperature database. At the cooler temperatures the σ_{abs} is changing more for each temperature step is the contributing factor for SRR< 1 x 10^4. Excluding the low-temperature edge, the interpolation successfully returns a SRR > 1 x 10^4. The increased in SRR shown in Figure 4.12 is attributed to the fact that the σ_{abs} changes less as temperature increases.

4.4.3 $\sigma_{abs}(X_{user})$ interpolation study

Finally, we evaluated the ability for 2D concentration interpolation. Spectra of varying molar

concentrations of H_2O 1 - 20%, CO_2 0 – 20%, with balance N_2, were simulated using a Voigt

lineshape at fixed pressure P = 25 bar, temperature T = 1000 K, spectral resolution of

0.0001 cm^{-1}, and path length L = 152.4 cm.

Using HITEMP2010 [23] parameters for line strength, line position, and lower state

energy spectra are simulated with a line strength cutoff of 1 x 10^{-21} cm^{-2} atm^{-1}. The cutoff is used

to isolate two nearby transitions in the wavenumber range of 7423 – 7429 cm^{-1}. Unfortunately,

HITEMP2010 only provides broadening parameters for H_2O and Air. In order to properly

simulate H_2O-, CO_2-, and N_2-perturbed H_2O, Voigt broadening parameters γ_{H2O-N2}, $\gamma_{H2O-H2O}$,

$\gamma_{H2O-CO2}$, and their associated temperature exponents $n_{\gamma N2}$, $n_{\gamma H2O}$, $n_{\gamma CO2}$ measured and presented

by Goldenstien in Table 4 [41] were used. The 4029.52 cm^{-1} transition parameters are arbitrarily

assigned to the 7426.129 cm^{-1} transition and the 4041.92 cm^{-1} transition parameters are

arbitrarily assigned to the 7426.593 cm^{-1}. Temperature-dependent broadening parameters were

calculated at 1000 K because at this temperature $\gamma_{H2O-H2O}$ and $\gamma_{H2O-CO2}$ are most different,

providing a challenging test for the interpolation algorithm.

A linear concentration spacing function was chosen for both H_2O and CO_2. An 8 x 8

matrix is created with rows of H_2O concentrations and columns of CO_2 concentrations. A 2D

spline interpolation was performed. Figure 4.13 represents an example of the absorbance signals

of the interpolated (top, solid black) and simulated reference (top, dashed red) along with the

residual (bottom), corresponding to the gas composition mole fractions interpolated σ_{abs} (red dot)

as shown in Figure 4.14. This example has a SRR = 1.2 x 10^4, and the σ_{abs} was interpolated as

mole fraction of $X_{H2O} = 0.0633$ and $X_{CO2} = 0.0236$ surrounded by database σ_{abs}'s with mole

fractions of $(X_{H2O} = 0.03714,\ X_{CO2} = 0)$, $(X_{H2O} = 0.03714,\ X_{CO2} = 0.0286)$, $(X_{H2O} = 0.0643,$ $X_{CO2} = 0)$ and $(X_{H2O} = 0.0643\ X_{CO2} = 0.0286)$. All interpolated spectra at each pressure have a SSR computed in the same manner as Equation 2.1.
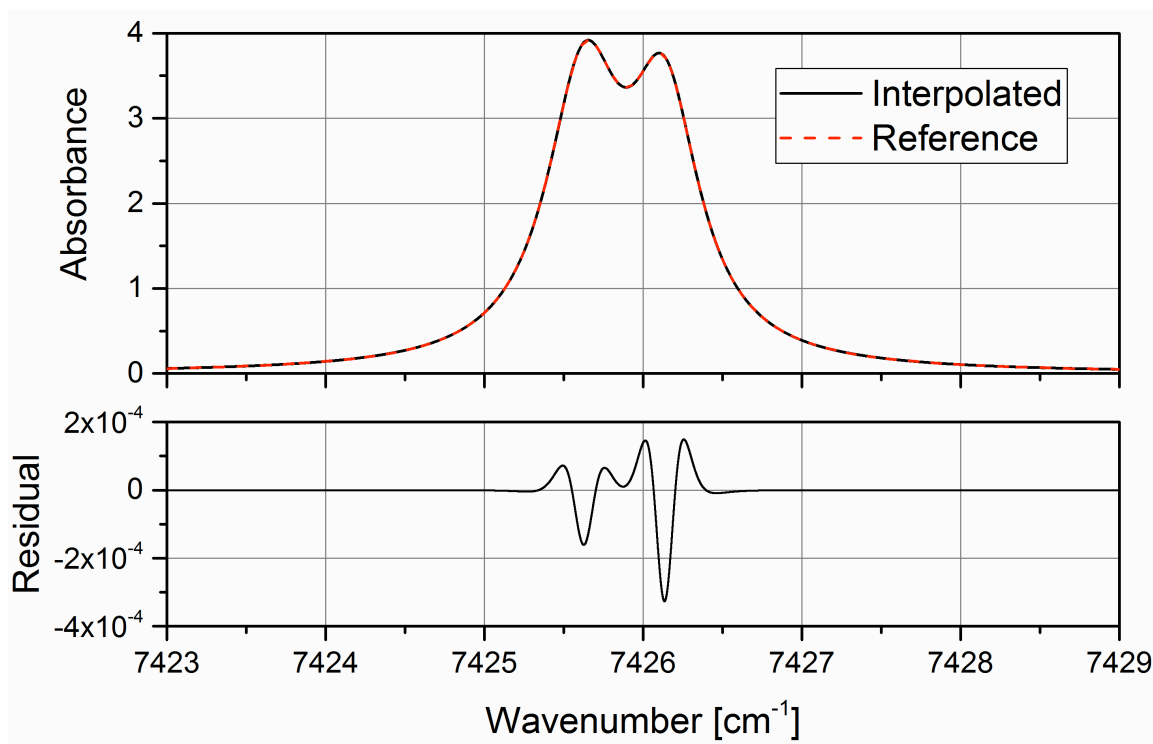
Figure 4.13 Concentration interpolation study. Top shows simulated reference spectra, red dash, compared to interpolated spectra, solid black. Bottom shows residual for two transitions with T = 1000 K, P = 25 bar, $X_{H2O} = 0.064$, and $X_{CO2} = 0.024$.

The SRR for all interpolated spectra at various mole fractions of X_{H2O} $0.01 - 0.2$ and of X_{CO2} $0 - 0.2$ is shown in Figure 4.12 as a 1D array.
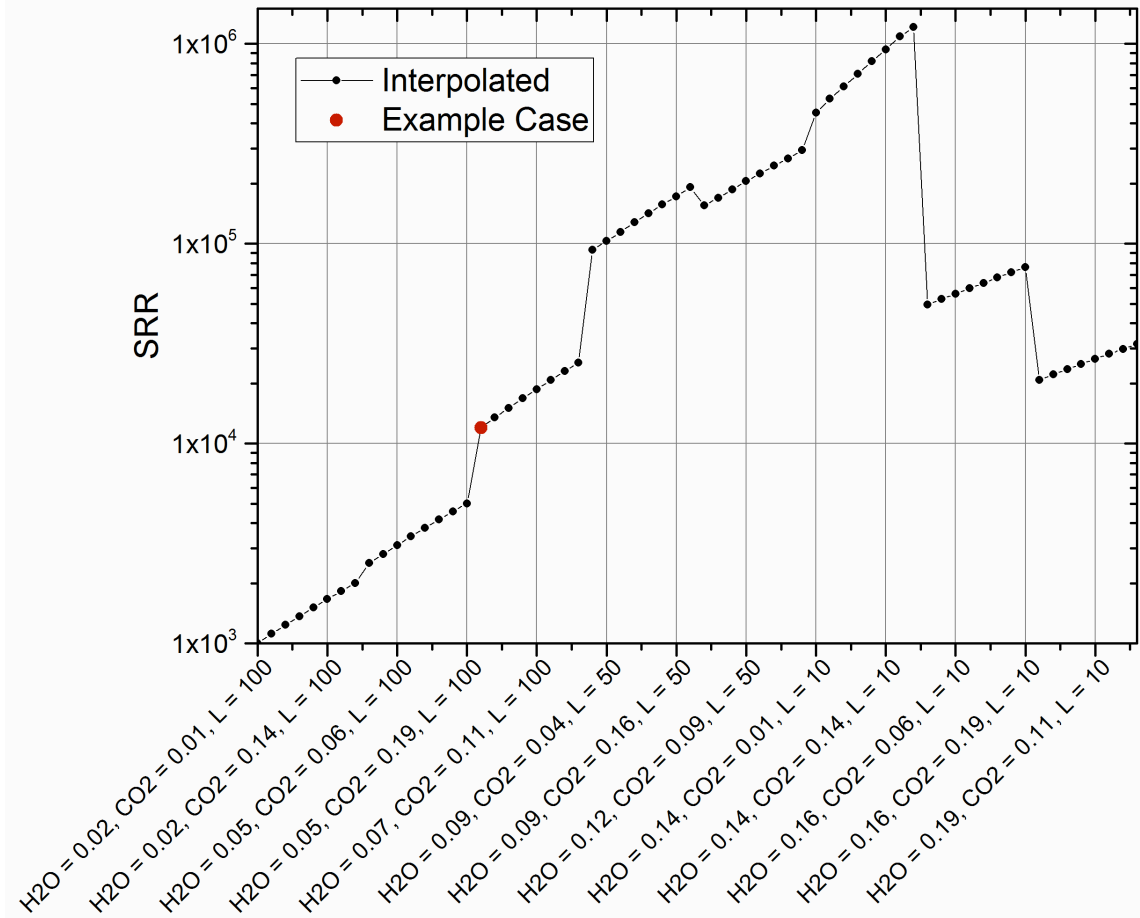
Figure 4.14 SRR for interpolated σ_{abs} with varied concentrations of H_2O and CO_2. Example case represents a SRR = 1.2 x 10^4 T = 1000 K, P = 25 bar, X_{H2O} = 0.064, and X_{CO2} = 0.024.

Once again, by using the spline interpolation some performance is lost near the edges of studied concentration region, most notably at the lowest concentrations of H_2O. Lower performance is found at $X_{H2O} < 0.06$ where the SRR > 1 x 10^3, while at $X_{H2O} > 0.06$ the SRR is > 1 x 10^4. Excluding the left edge, the interpolation successfully returns a SRR > 1 x 10^4.

4.5 Conclusions

Both Line-by Line and σ_{abs} approaches have benefits and detriments, however in the near term we believe the σ_{abs} approach is most appropriate. Our group will soon possess the ability to measure reference spectra at conditions discussed above. There is no replacement for the understanding of fundamental water spectra and for that a LBL approach is necessary. For the LBL approach research needs to be invested in developing the necessary physics models, parameter extraction techniques. The σ_{abs} approach allows for reference grade spectra to be immediately useful for researchers to perform thermodynamic measurements (Pressure, Temperature, and Molar Composition) with water spectra. Individual interpolation methods perform well and it is known that multivariate interpolation of splines with n dimensions relies on the tensor product which does not introduce additional error. I have determined that high-temperature H_2O is better suited to the absorption cross-section approach. H_2O near 2120 K behaves more like the Figure 4.2B case than the Figure 4.2A case.

Chapter 5. Future Work

5.1   Furnace operation

A high-temperature furnace, enclosed in a pressure vessel, will be used to create combustion-like conditions to measure spectra. The furnace will be designed in the same spirit as Melin [42] has done. Pressure will be balanced inside the test section and inside the furnace. A total of 64 combined H_2O/ CO_2/ N_2 gas mixtures will be tested. Each mixture will be prepared in an external stainless chamber. The chamber will be heated to 220 °C at the bottom and 200 °C at the top. The 200 °C value prevents condensation of water even at partial pressures up to 20 bar. The 20 °C gradient drives a convective flow within the chamber to thoroughly mix the gas before it is introduced into the cell. The programmatic cell operation is illustrated in Figure 5.1.
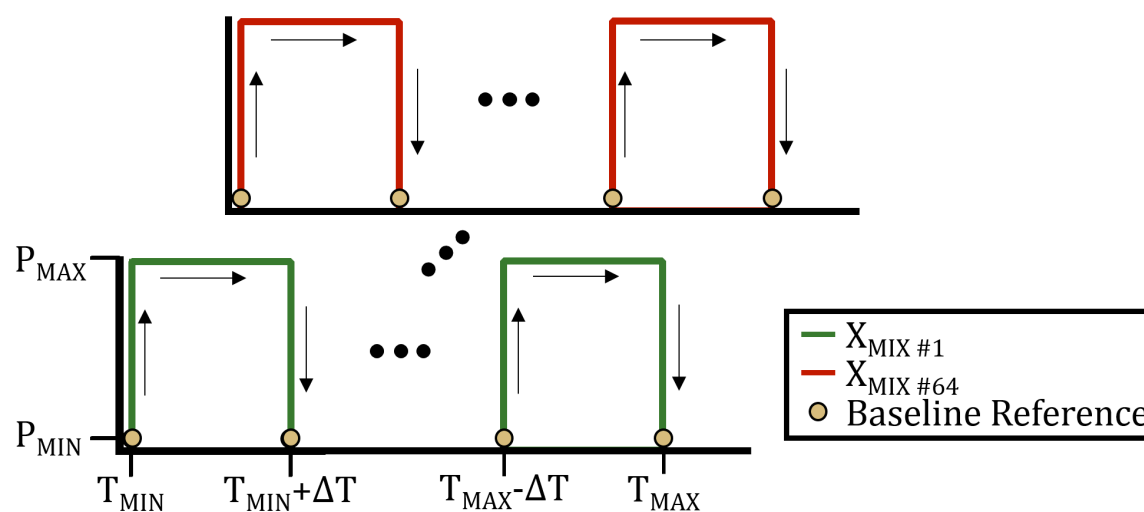
Figure 5.1 Cell operating diagram: beginning with mixture 1 at T_{min}, P_{min}, pressure is incremented to P_{max}, then temperature is incremented, then pressure is decremented to P_{min}, then temperature is incremented, etc. until the mixture is changed to mixture 2, etc. and finally to mixture 64.

The cell will be initially evacuated and at held at a temperature $T_{min;}$ a reference (baseline) spectrum is recorded at this condition. The first H_2O-CO_2-N_2 gas mixture (mixture #1) will be

prepared in the heated chamber at a pressure of ~ 120 bar. A small fraction of the mixture will be delivered to the cell, sufficient to raise the pressure to P_{min} (0.5 bar). After equilibrium is reached, a spectrum is recorded. Additional mixture will be delivered to increment the cell pressure to the second test pressure (89 pressure steps + 1 baseline pressure = 90 total pressures). After equilibrium, a spectrum will be recorded. The process repeats until P_{max} (50 bar) is reached. Then the cell temperature will be incremented to the second test temperature (of 15 total temperatures). After equilibrium, a spectrum will be recorded. Then the pressure will be decremented incrementally until P_{min} is reached, each time pausing to record a spectrum. Then the cell will be evacuated and a new reference spectrum will be recorded. Then the temperature will be incremented to the third test temperature. Operation continues in this fashion until all temperatures and pressures have been measured for mixture 1. Then the mixture will be changed to mixture 2, and so on until mixture 64 is tested. The entire test time will be anticipated to be about a 1 year, but is likely to be reduced with further refinement of the test matrix.

5.2 Database inquiry

Recording absorption cross-section spectra is only a portion of the future goal, another key aspect will be to ensure the ability for researchers, outside Sanders group and across the world, access to this database and the interpolation algorithm. A web-based system will be implemented to provide worldwide inquiry of the proposed HTPD. A suggested method of inquiry is further developed below.

Step 1 the user will input the path length, range of wavenumbers to be covered along with the thermodynamic conditions T_{user}, P_{user}, X_{user_H2O} and X_{user_CO2}. The inquiry system will then identify the measured σ_{abs} thermodynamic conditions that are closest to the user-entered conditions to use as σ_{abs} thermodynamic database values T_{DB}, P_{DB}, X_{DB_H2O} and X_{DB_CO2}.

Step 2, the case of gas composition, a page of 16 σ_{abs} with various mole fractions surounding the user defined values of X_{user_H2O} and X_{user_CO2} are selected. Each page contains σ_{abs}, shown as tan datapoint, with rows of varied X_{H2O} and columns of varied X_{CO2}. The 16 σ_{abs} are outlined in black in Figure 5.2. These mole fractions are set with fixed setps $\Delta X_{H2O,}$ and ΔX_{CO2}.

Step 3 we interpolate over this page of gas compositions using a 2D spline to create an $\sigma_{abs}(\nu, X_{user\_H2O,} X_{user\_CO2,} T_{DB,} P_{DB})$, shown with a red outline in Figure 5.2.
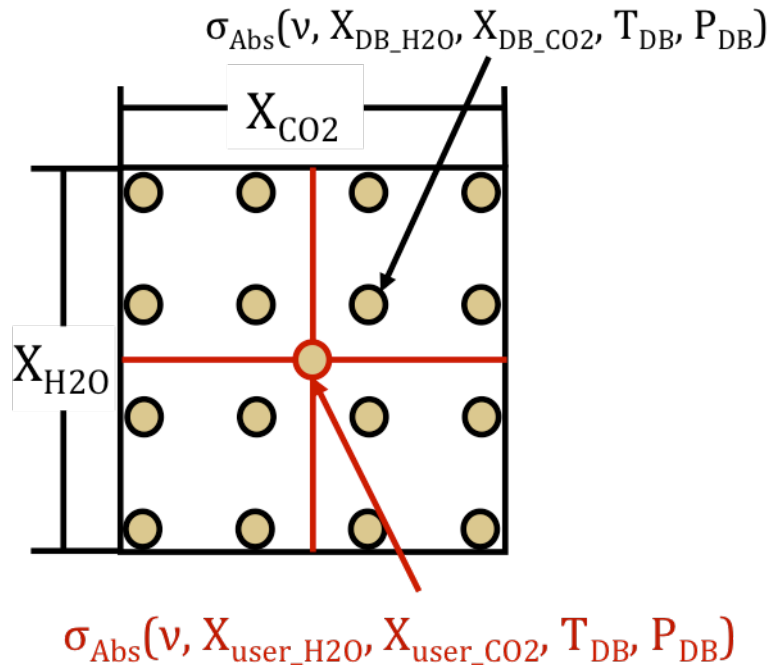
Figure 5.2 Page of σ_{abs} with various gas compositions. Each page contains rows of varied X_{H2O} and colunms of varied X_{CO2} σ_{abs} with constant temperature (T_{DB}) and pressure (P_{DB}). The red outlined datapoint represents the interpolated gas composition, $\sigma_{abs}(\nu, X_{user\_H2O}, X_{user\_CO2}, T_{DB}, P_{DB})$.

Step 4 we repeat step 3 (2D interpolation over a page of 16 σ_{abs} with various mole fractions) three times using three other temperatures $T_{DB}+\Delta T$, $T_{DB}-\Delta T$, & $T_{DB}-2\Delta T$. The four σ_{abs} would have constant pressure (P_{DB}) and constant interpolated mole fraction (X_{user_H2O}, X_{user_CO2}) which will be called X_{user}. These four pages of σ_{abs} form a volume that would then be

interpolated over to define a $\sigma_{abs}(v, X_{user\_H2O}, X_{user\_CO2}, T_{user}, P_{DB})$. Each σ_{abs} page of interpolated gas compositions at four temperatures would be formed into a volume. The volume would be interpolated to find the $\sigma_{abs}(v, X_{user\_H2O}, X_{user\_CO2}, T_{user}, P_{DB})$ for a total of 5 interpolations. The interpolated $\sigma_{abs}(v, X_{user}, T_{user}, P_{DB})$ is outlined in blue, as shown in Figure 5.3.
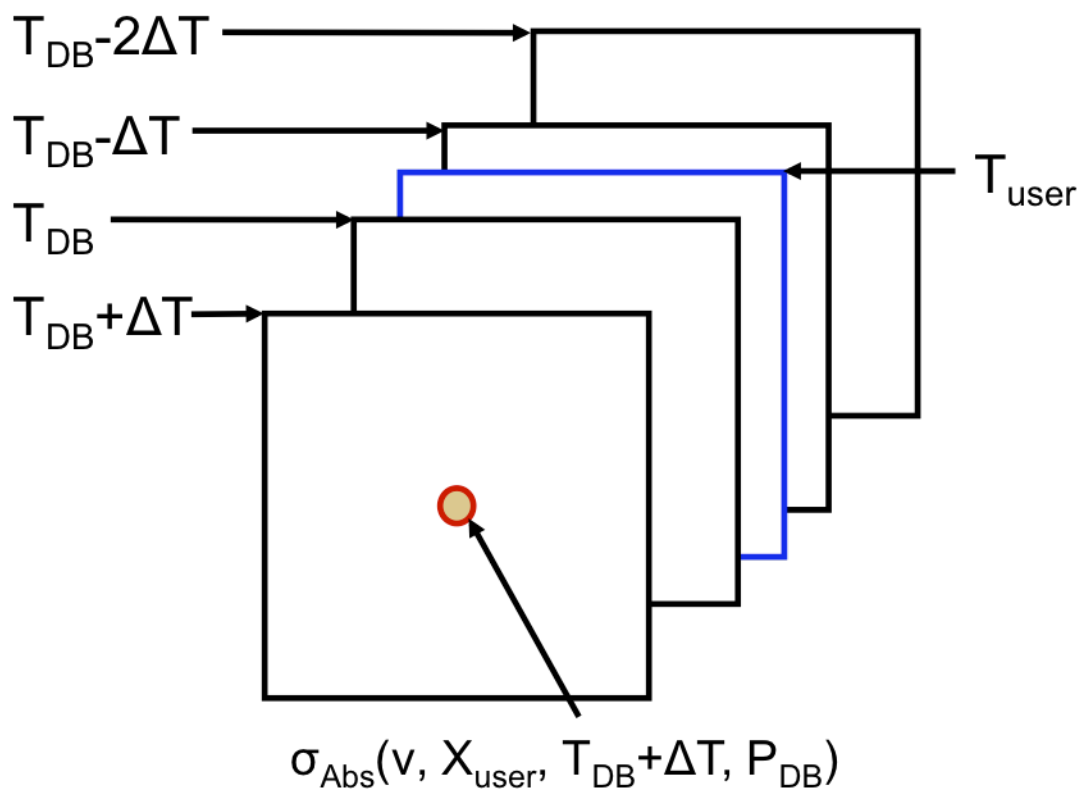
Figure 5.3 Volume of σ_{abs} with various temperatures and a fixed interpolated mole fraction. Each volume contains pages of varied temperature σ_{abs} with constant molar composition (X_{user}) and pressure (P_{DB}). The blue outlined page represents the interpolated $\sigma_{abs}(v, X_{user}, T_{user}, P_{DB})$.

Step 5 we repeat step 4 (1D interpolation over a volume of 4 σ_{abs} with various temperatures) three times using three other pressures $P_{DB}+\Delta P$, $P_{DB}-\Delta P$, & $P_{DB}-2\Delta P$. The four σ_{abs} would have constant temperature (T_{user}) and constant interpolated mole fraction (X_{user}). These four σ_{abs} form a library that would then be interpolated over to define a $\sigma_{abs}(v, X_{user}, T_{user}, P_{user})$. Each σ_{abs} volume of interpolated gas compositions and temperatures at four pressures would be

formed into a library, bring the interpolation total to 20. The library would then be interpolated to find the $\sigma_{abs}(v, X_{user}, T_{user}, P_{user})$ for a grand total of 21 interpolations. The σ_{abs} library is interpolated through and the result $\sigma_{abs}(v, X_{user}, T_{user}, P_{user})$ is outlined in green, as shown in Figure 5.4.
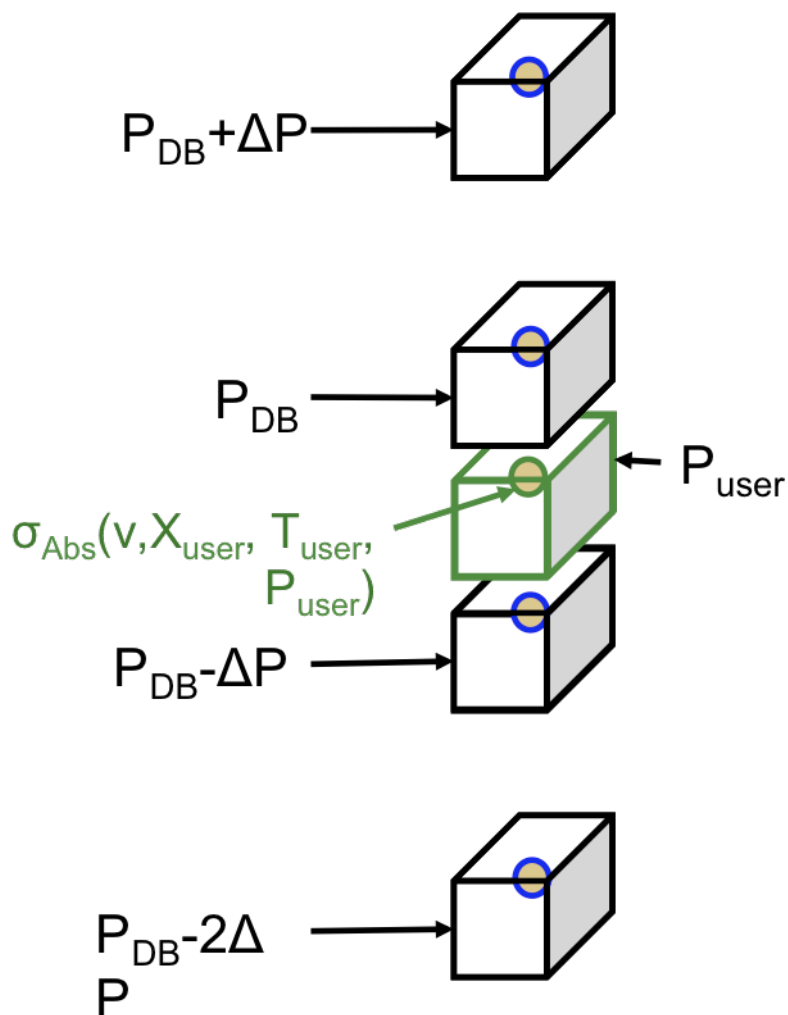
Figure 5.4 Library of σ_{abs} with various pressures and a fixed interpolated temperature and mole fraction. Each library contains volumes of varied pressure σ_{abs} with constant molar composition (X_{user}) and temperature (T_{user}). The green outlined volume represents the interpolated $\sigma_{abs}(v, X_{user}, T_{user}, P_{user})$.

All thermodynamic condition step sizes (ΔX_{H2O}, ΔX_{CO2}, ΔT) are linear except for ΔP which is a hybrid pressure step shown in Equation 4.4.

To recap, each σ_{abs} library consists of four constant pressure σ_{abs} volumes that are interpolated to recover the user pressure, shown in Figure 5.4, each constant pressure volume contains four constant temperature σ_{abs} pages that are interpolated over to recover the user temperature, as shown in Figure 5.3, and each constant temperature page contains four rows of constant H_2O molar concentrations and four columns of constant CO_2 molar concentrations that are interpolater to recover user mole fraction, as shown in Figure 5.2. The result of the 21 interpolated absorption cross-sections would be $\sigma_{abs}(v, X_{user}, T_{user}, P_{user})$. This σ_{abs} would then be scaled by path length, number density, and absorber mole fraction to convert to absorbance, and output to the user.

References

[1] Fateev, A., and Clausen, S., 2008, "On-line non-contact gas analysis," Report No. 978-87-550-3659-8, Danmarks Tekniske Universitet, Risø Nationallaboratoriet for Bæredygtig Energi.

[2] Smith, C. H., Goldenstein, C. S., and Hanson, R. K., 2014, "A scanned-wavelength-modulation absorption-spectroscopy sensor for temperature and H2O in low-pressure flames," Measurement Science & Technology, 25(11).

[3] Gryvnak, D. A., and Burch, D. E., 1965, "Optical and infrared properties of Al2O3 at elevated temperatures," Optical Society of America -- Journal, 55(6), pp. 625-629.

[4] Wang, Z., and Sanders, S., 2015, "Toward single-ended absorption spectroscopy probes based on backscattering from rough surfaces: H2O vapor measurements near 1350 nm," Applied Physics B, 121(2), pp. 187-192.

[5] Berg, T., Thiele, O., Seefeldt, S., and Vanhaelst, R., 2013, "Measurement of in-cylinder mixture formation by optical indication," MTZ worldwide, 74(6), pp. 26-30.

[6] Yang, D., Thomas, M. E., Tropf, W. J., and Kaplan, S. G., "Infrared refractive index measurements using a new method," pp. 42-52.

[7] Schlosser, E., Fernholz, T., Teichert, H., and Ebert, V., 2002, "In situ detection of potassium atoms in high-temperature coal-combustion systems using near-infrared-diode lasers," Spectrochimica Acta A, 58A(11), pp. 2347-2359.

[8] Ma, L., Li, X., Sanders, S. T., Caswell, A. W., Roy, S., Plemmons, D. H., and Gord, J. R., 2013, "50-kHz-rate 2D imaging of temperature and H2O concentration at the exhaust plane of a J85 engine using hyperspectral tomography," Optics Express, 21(1), pp. 1152-1162.

[9] Witzel, O., Klein, A., Meffert, C., Wagner, S., Kaiser, S., Schulz, C., and Ebert, V., 2013, "VCSEL-based, high-speed, in situ TDLAS for in-cylinder water vapor measurements in IC engines," Optics Express, 21(17), pp. 19951-19951.

[10] Arroyo, M. P., and Hanson, R. K., 1993, "Absorption measurements of water-vapor concentration, temperature, and line-shape parameters using a tunable InGaAsP diode laser," Applied Optics, 32(30), pp. 6104-6116.

[11] Witzel, O., Klein, a., Wagner, S., Meffert, C., Schulz, C., and Ebert, V., 2012, "High-speed tunable diode laser absorption spectroscopy for sampling-free in-cylinder water vapor concentration measurements in an optical IC engine," Applied Physics B, 109(3), pp. 521-532.

[12] Kranendonk, L. A., An, X., Caswell, A. W., Herold, R. E., Sanders, S. T., Huber, R., Fujimoto, J. G., Okura, Y., and Urata, Y., 2007, "High speed engine gas thermometry by Fourier-domain mode-locked laser absorption spectroscopy," Optics Express, 15(23), pp. 15115-15115.

[13] Baer, D. S., Nagali, V., Furlong, E. R., Hanson, R. K., and Newfield, M. E., 1996, "Scanned- and fixed-wavelength absorption diagnostics for combustion measurements using multiplexed diode lasers," AIAA Journal, 34(3), pp. 489-493.

[14] Furlong, E. R., Mihalcea, R. M., Webber, M. E., Baer, D. S., and Hanson, R. K., 1999, "Diode-laser sensors for real-time control of pulsed combustion systems," AIAA Journal, 37(#6Ge Co,Corp Res & Dev,1 Res Circle,Bldg K1-Es,Room 109,Niskayuna,Ny 12309 ; Stanford Univ,Dept Mech Engn,High Temp Gasdynam Lab,Stanford,Ca 94305 English Article Bibliography Items: 29 Number of times cited: 0 (c) 1999 Inst. For Sci. Info), pp. 732-737.

[15] Spearrin, R. M., Ren, W., Jeffries, J. B., and Hanson, R. K., 2014, "Multi-band infrared CO2 absorption sensor for sensitive temperature and species measurements in high-temperature gases," Applied Physics B, 116(4), pp. 855-865.

[16] Karagiannopoulos, S., Cheadle, E., Wright, P., Tsekenis, S., and McCann, H., 2012, "Multiwavelength diode-laser absorption spectroscopy using external intensity modulation by semiconductor optical amplifiers," Applied optics, 51(34), pp. 8057-8067.

[17] Caswell, A. W., Roy, S., An, X., Sanders, S. T., Schauer, F. R., and Gord, J. R., 2013, "Measurements of multiple gas parameters in a pulsed-detonation combustor using time-division-multiplexed Fourier-domain mode-locked lasers," Applied optics, 52(12), pp. 2893-2904.

[18] An, X., Caswell, A. W., Lipor, J. J., and Sanders, S. T., 2015, "Optimized Wavelength Selection for Molecular Absorption Thermometry," Applied Spectroscopy, 69(4), pp. 464-472.

[19] Rieker, G. B., Li, H., Liu, X., Liu, J. T. C., Jeffries, J. B., Hanson, R. K., Allen, M. G., Wehe, S. D., Mulhall, P. A., Kindle, H. S., Kakuho, A., Sholes, K. R., Matsuura, T., and Takatani, S., 2007, "Rapid measurements of temperature and H2O concentration in IC engines with a spark plug-mounted diode laser sensor," Proceedings of the Combustion Institute, 31, pp. 3041-3049.

[20] Mattison, D. W., Jeffries, J. B., Hanson, R. K., Steeper, R. R., De Zilwa, S., Dec, J. E., Sjoberg, M., and Hwang, W., 2007, "In-cylinder gas temperature and water concentration measurements in HCCI engines using a multiplexed-wavelength diode-laser system: Sensor development and initial demonstration," Proceedings of the Combustion Institute, 31(1), pp. 791-798.

[21] Sanders, S. T., Baldwin, J. A., Jenkins, T. P., Baer, D. S., and Hanson, R. K., 2000, "Diode-laser sensor for monitoring multiple combustion parameters in pulse detonation engines," Proceedings of the Combustion Institute, 28, pp. 587-594.

[22] Rothman, L. S., Gordon, I. E., Babikov, Y., Barbe, A., Benner, D. C., Bernath, P. F., Birk, M., Bizzocchi, L., Boudon, V., Brown, L. R., Campargue, A., Chance, K., Cohen, E. A., Coudert, L. H., Devi, V. M., Drouin, B. J., Fayt, A., Flaud, J. M., Gamache, R. R., Harrison, J. J., Hartmann, J. M., Hill, C., Hodges, J. T., Jacquemart, D., Jolly, A., Lamouroux, J., LeRoy, R. J., Li, G., Long, D. A., Lyulin, O. M., Mackie, C. J., Massie, S. T., Mikhailenko, S., Müller, H. S. P., Naumenko, O. V., Nikitin, A. V., Orphal, J., Perevalov, V., Perrin, A., Polovtseva, E. R.,

Richard, C., Smith, M. A. H., Starikova, E., Sung, K., Tashkun, S., Tennyson, J., Toon, G. C., Tyuterev, V. G., and Wagner, G., 2013, "The HITRAN2012 Molecular Spectroscopic Database," Journal of Quantitative Spectroscopy and Radiative Transfer, null(null).

[23] Rothman, L. S., Gordon, I. E., Barber, R. J., Dothe, H., Gamache, R. R., Goldman, A., Perevalov, V. I., Tashkun, S. A., and Tennyson, J., 2010, "HITEMP, the high-temperature molecular spectroscopic database," Journal of Quantitative Spectroscopy and Radiative Transfer, 111(15), pp. 2139-2150.

[24] Rieker, G. B., Giorgetta, F. R., Swann, W. C., Sinclair, L. C., Cromer, C. L., Baumann, E., Coddington, I. R., and Newbury, N. R., "Dual-Frequency Comb Measurements of Atmospheric Absorption: Comparison with HITRAN Database Parameters," Proc. CLEO: 2015, Optical Society of America, p. SW1G.2.

[25] Alberti, M., Weber, R., Mancini, M., Fateev, A., and Clausen, S., 2015, "Validation of HITEMP-2010 for carbon dioxide and water vapour at high temperatures and atmospheric pressures in 450–7600 cm−1 spectral range," Journal of Quantitative Spectroscopy and Radiative Transfer, 157, pp. 14-33.

[26] Kranendonk, L. A., Caswell, A. W., and Sanders, S. T., 2007, "Robust method for calculating temperature, pressure and absorber mole fraction from broadband spectra," Applied Optics, 46(19).

[27] Farooq, A., Jeffries, J. B., and Hanson, R. K., 2010, "High-pressure measurements of CO2 absorption near 2.7 m: line mixing and finite duration collision effects," Journal of Quantitative Spectroscopy and Radiative Transfer, 111(7-8), pp. 949-960.

[28] Goldenstein, C. S., and Hanson, R. K., 2015, "Diode-laser measurements of linestrength and temperature-dependent lineshape parameters for H2O transitions near 1.4 μm using Voigt, Rautian, Galatry, and speed-dependent Voigt profiles," Journal of Quantitative Spectroscopy and Radiative Transfer, 152, pp. 127-139.

[29] Ouyang, X., and Varghese, P. L., 1990, "Selection of spectral lines for combustion diagnostics," Applied optics, 29(33), pp. 4884-4890.

[30] Zhou, X., Jeffries, J. B., and Hanson, R. K., 2005, "Development of a fast temperature sensor for combustion gases using a single tunable diode laser," Applied Physics B, 81(5), pp. 711-722.

[31] Bolshov, M. A., Kuritsyn, Y. A., Liger, V. V., and Mironenko, V. R., 2011, "Development of diode laser absorption spectroscopy method for determining temperature and concentration of molecules in remote object," Optics and Spectroscopy, 110(6), pp. 848-856.

[32] Whitney, J. M., Takami, K., Sanders, S. T., and Okura, Y., 2011, "Design of System for Rugged, Low-Noise Fiber-Optic Access to High-Temperature, High-Pressure Environments," IEEE Sensors Journal, 11(12), pp. 3295-3302.

[33] Schulze, G., Jirasek, A., Yu, M. M. L., Lim, A., Turner, R. F. B., and Blades, M. W., 2005, "Investigation of selected baseline removal techniques as candidates for automated implementation," Applied Spectroscopy, 59(5), pp. 545-574.

[34] Kranendonk, L. A., Caswell, A. W., Hagen, C. L., Neuroth, C. T., Shouse, D. T., Gord, J. R., and Sanders, S. T., 2009, "Temperature measurements in a gas-turbine-combustor sector rig using swept-wavelength absorption spectroscopy," Journal of Propulsion and Power, 25(4), pp. 859-863.

[35] Kranendonk, L. A., and Sanders, S. T., 2005, "Optical design in beam steering environments with emphasis on laser transmission measurements," Applied Optics, 44(31), pp. 6762-6772.

[36] Barber, R. J., Tennyson, J., Harris, G. J., and Tolchenov, R. N., 2006, "A high-accuracy computed water line list," Monthly Notices of the Royal Astronomical Society, 368(3), pp. 1087-1094.

[37] Tennyson, J., Bernath Peter, F., Campargue, A., Császár Attila, G., Daumont, L., Gamache Robert, R., Hodges Joseph, T., Lisak, D., Naumenko Olga, V., Rothman Laurence, S., Tran, H., Zobov Nikolai, F., Buldyreva, J., Boone Chris, D., De Vizia Maria, D., Gianfrani, L., Hartmann, J.-M., McPheat, R., Weidmann, D., Murray, J., Ngo Ngoc, H., and Polyansky Oleg, L., 2014, "Recommended isolated-line profile for representing high-resolution spectroscopic transitions (IUPAC Technical Report)," Pure and Applied Chemistry, p. 1931.

[38] Sharpe, S. W., Johnson, T. J., Sams, R. L., Chu, P. M., Rhoderick, G. C., and Johnson, P. A., 2004, "Gas-Phase Databases for Quantitative Infrared Spectroscopy," Applied Spectroscopy, 58(12), pp. 1452-1461.

[39] Vidler, M., and Tennyson, J., 2000, "Accurate partition function and thermodynamic data for water," Journal of Chemical Physics, 113(21), pp. 9766-9771.

[40] Fischer, J., Gamache, R. R., Goldman, A., Rothman, L. S., and Perrin, A., "Total internal partition sums for molecular species in the 2000 edition of the HITRAN database," Journal of Quantitative Spectroscopy and Radiative Transfer, 82(1–4), pp. 401-412.

[41] Goldenstein, C. S., Jeffries, J. B., and Hanson, R. K., 2013, "Diode laser measurements of linestrength and temperature-dependent lineshape parameters of H2O-, CO2-, and N2-perturbed H2O transitions near 2474 and 2482 nm," Journal of Quantitative Spectroscopy and Radiative Transfer, 130, pp. 100-111.

[42] Melin, S. T., and Sanders, S. T., 2016, "Gas cell based on optical contacting for fundamental spectroscopy studies with initial reference absorption spectrum of H2O vapor at 1723 K and 0.0235 bar," Journal of Quantitative Spectroscopy & Radiative Transfer, 180, pp. 184-191.